Chapter 14

Investigation of Site Response in Urban Areas by Using Earthquake Data and Seismic Noise

(Version January 2012; DOI: 10.2312/GFZ.NMSOP-2_ch14)

Stefano Parolai

Helmholtz Centre Potsdam, GFZ German Research Centre for Geosciences, Department 2:Physics of the Earth, Section 2.1: Earthquake Risk and Early Warning, Telegrafenberg, 14473 Potsdam, Germany, E-mail: parolai@gfz-potsdam.de

"It is certainly not enough to have softwares available to all so that all are musicians."
Angelo Bergamini

14.1 Introduction

The distribution of damages due to recent earthquakes have shown that the effects of local geology on ground shaking represent an important factor in engineering seismology. Figure 14.1, schematically shows that when an earthquake occurs, waves generated at the source propagate through the Earth (generally with decreasing amplitude with distance). When two

nearby sites are located on the top of different materials, the ground shaking they experience can be very different. These differences might be very important considering that (1) buildings can react to the input ground motion emphasising shaking depending on their frequency of oscillation, and (2) that they can even redistribute energy back to the Earth due to scattering and diffraction of seismic waves when interacting with their foundations and acting as a source while shaking.
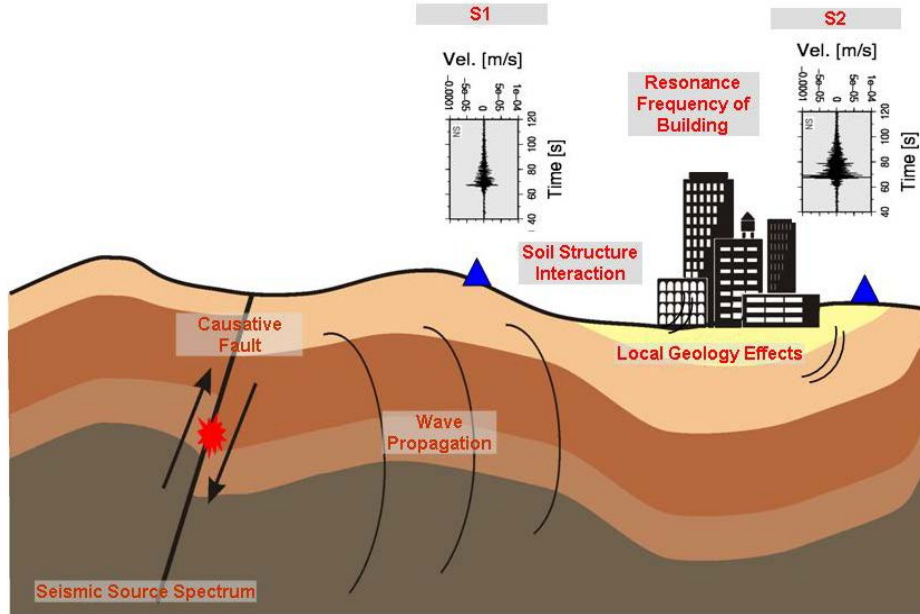

Fig. 14.1 Simplified representation showing seismic wave propagation after an earthquake. Blue triangles indicate stations located over different near surface geological material (S1 on a rock site and S2 on soft quaternary material) experiencing different ground motion.

The modification of the ground motion due to the Earth structure below the site can be related to different factors (e.g., Safak, 2001) (Fig. 14.2). In general, the main factor is the impedance contrast (see Chapter 2, subsection 2.5.4.1) between the soft sedimentary cover (with low density ρ_1 and wave propagation velocity v_1) and the bedrock (with high density ρ_2 and wave propagation velocity v_2). The impedance contrast $c=(v_2\,\rho_2)/(v_1\,\rho_1)$ determines how strongly the waves at particular frequencies (the fundamental resonance frequency and the higher harmonics) are multi-reflected within the soft layer, thus trapping the wave energy within the layer (1-D effect). Quantitatively, and under the simplified assumption of vertical propagation of S waves, the modulus of the 1-D site amplification function *H(f)* can be described by the following relation:

$$|H(f)| = \left(\frac{(1+r)^2}{1+2r\cos(4\pi f\tau)+r^2}\right)^{\frac{1}{2}},$$

(14.1)

where τ is the travel time of the S waves in the soft sedimentary layer and $r=(\rho_2 v_2-\rho_1 v_1)/(\rho_2 v_2+\rho_1 v_1)$ is the reflection coefficient that is clearly related to the impedance contrast *c*. The maximum of *H(f)* is obtained when $\cos(4\pi f\tau)$ is equal to -1 that is when $f = 1/(4\tau)$. This value of *f* is defined as the fundamental resonance frequency f_0. From the previous

consideration it follows the well know relationship $f_0 = v_1/(4h_1)$ where h_1 is the thickness of the soft sedimentary layer.

The site response (here represented by the shape of the Fourier spectra amplitude ratio between the surface recording and the input ground motion at the bedrock) is then determined by the S-wave velocity and the thickness of the sedimentary cover layer, which determine the frequencies that are affected by amplification, while the impedance contrast controls the amplification level. The quality factor Q (see Chapter 2, subsection 2.5.4.2) in the soft sedimentary cover influences the decay of the site response with increasing frequency.

 Other effects like focusing, diffraction of body waves at the edges of sedimentary basins (2-D or 3-D effects) and scattering should also be taken into account. Sites located on pronounced (with respect to wavelength) topographic relief can also suffer significant amplification of ground motion. Importantly, in the case of strong ground motion the soil may behave non-linearly. In particular, the frequency of resonance of soil tends then to decrease and the damping to increase. Due to pore pressure increase and dilatancy high frequency spikes in ground motion are occasionally observed (Bonilla et al., 2005).

Thus, assessing the amplification/deamplification and lengthening of seismic ground motion due to superficial geology is of primary importance for earthquake microzonation studies. In the past few decades, the evaluation of site effects has attracted growing attention. In particular, due to the increasing importance of reliable seismic hazard assessment in large urban areas (e.g., Istanbul, Santiago de Chile), large efforts has been devoted to the development of tools for site effect estimation that allow large areas to be covered at limited costs.
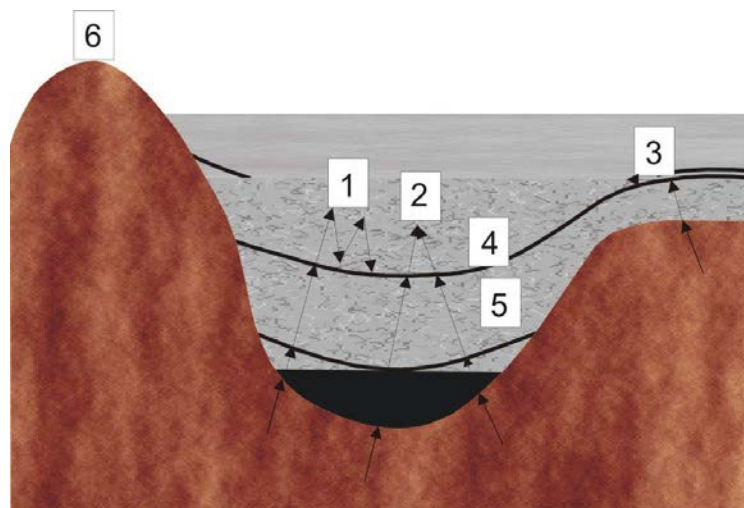

Fig. 14.2 Local features and effects that can modify the ground motion: 1) Resonance due to impedance contrasts; 2) Focusing due to subsurface topography; 3) Body waves converted to surface waves; 4) Water content; 5) Heterogeneity of the Earth medium; 6) Surface topography (Safak, 2001).

Site effects can be estimated by means of numerical simulations and experimental methods. The former range from simple 1-D numerical calculations to methods that consider complex phenomena and model geometry. In general, the experimental methods are subdivided into two categories: reference site and non-reference site techniques (see, e.g., Bard, 1995).

Borcherdt (1970) was the first to propose the reference site method (RSM) that consists in comparing records at nearby sites, using one as the reference site. It is assumed that records from the reference site (in general a station installed on outcropping hard rock) contain the same source and propagation effects as records from the other sites. Therefore, differences observed between the sites are explained as being due to local site effects. This method is generally applicable only to data from dense, local station deployments of arrays (see also Chapter 9 of this Manual). Andrews (1986) extended this method to large networks. He proposed to separate the contribution of the path, the source, and the site by means of an inversion scheme termed the generalized inversion technique (GIT). Since in general the site amplification at a reference (hard rock) site is set to unity, this approach provides results analogous to those obtained by the RSM method.

However, the major drawback of these methods is that a suitable reference site may not always be available (Steidl et al., 1996), because also rock sites might have their own response. Furthermore, being rock site often located on hills, topographic effects (due to the geometry of the Earth surface, the weathering of the shallow rock layers etc.) cannot be easily ruled out . In order to overcome this disadvantage, non-reference site techniques such as the horizontal-to-vertical (H/V) spectral ratio method are widely used, although they provide only partial information about the site response. Nogoshi and Igarashi (1970) first introduced this technique, but Nakamura (1989) developed it further as a tool for estimating the site response of S waves. Originally, it was proposed for interpreting ambient seismic noise measurements (NHV). Lermo and Chavez-Garcia (1993) applied the H/V technique to the S waves of earthquake recordings (EHV) and developed a theoretical background for the technique using numerical modelling of SV waves.

The comparison of site responses obtained with reference and non-reference site techniques (e.g. Field and Jacob, 1995; Bonilla et al., 1997; Riepl et al., 1998; Triantafyllidis et al., 1999; Parolai et al., 2000; 2001a; 2004) has shown that RSM and EHV usually provide site responses with similar shapes when the S-wave part of the seismogram is used. The fundamental resonance frequency of a site is consistently estimated by both methods. However, they can provide different levels of amplification, in particular at frequencies higher than the fundamental one. Parolai and Richwalski (2004) showed, by means of numerical simulations, that differences between the RSM and the EHV results are caused by the effect of waves that have been converted at the bedrock depth and are included in the analyzed record time windows. In particular, due to the S-to-P conversion, a deamplification at frequencies higher than the fundamental one is observed in the EHV ratio for S-waves.

NHV has been shown to provide (e.g., Haghshenas et al., 2008) a good estimate of the fundamental resonance frequency of the S waves, but it underestimates the level of amplification with respect to GIT and RSM. Also, by using the P-wave part of the seismograms, the RSM and EHV methods have been found to provide consistent results only in some cases.

In the following, the development, testing and application of techniques for site effect estimation is outlined with special attention to studies carried out in large urban areas. First, the most popular methods for site effects investigation in urban area are described. Second, the use of seismic noise as an optimal tool for investigating the subsoil structure in urban areas will be illustrated. Not described are here other subsoil investigation methods based on active sources such as SASW (Stokoe et al., 1994), MASW (Park et al., 1999) and REMI (Louie 2001). Finally, based on the experience gained in the application of empirical

techniques to large urban areas, recommendations are given on how to estimate best site effects in different environments.

The intention of this chapter is to provide an overview of the work carried out during past and ongoing activities, with an emphasis on personal practical experience. Thus, this chapter may not appear to some readers to be a comprehensive review of the huge amount of significant literature that has been published in this field. If so, the author apologises for this.

14.2 Empirical methods (earthquake based)

The empirical methods can be classified into two categories: reference site and non reference site techniques. While the former requires the availability of a station installed on a hard rock outcrop (the reference site), the latter assumes that one of the components of the ground motion (generally the vertical one) provides the input ground motion at the bedrock (see for more details 14.2.2). This assumption is mainly based on the empirical observation of similar amplitude of the horizontal and vertical component of ground motion in borehole recordings and on the presumed lack of amplification of the latter one.

14.2.1 Reference site techniques

Reference site techniques can be used by taking the direct spectral ratio of the same component of ground motion recorded at two nearby stations (Standard Spectral Ratio SSR) (Fig. 14.3) or by deriving the site response via an inversion procedure (generalized inversion technique GIT). Generally, S-wave or P-wave signal windows are extracted from the seismograms starting before the phase arrival and ending either when a certain amount of energy is reached or after a pre-fixed amount of seconds. The selected time series are corrected for the instrumental response and the trend in the data. The two horizontal components can be analysed separately or combined. The vectorial sum or the root means square of the two horizontal components is often used in the analysis. Both ends of the selected signal window are tapered (for example with 5% cosine functions) and then the Fast Fourier Transform (FFT) calculated. Tapering is necessary to suppress spectral leakage before calculating the FFT (see IS 14.1). The resulting spectra are smoothed by using running time windows (preferably equally spaced on a logarithmic scale). The analyses are performed considering frequencies with a signal-to-noise (SNR) ratio larger than a certain threshold (generally at least 3), estimated by considering the Fast Fourier Transform (FFT) of a noise window as wide as the signal window.
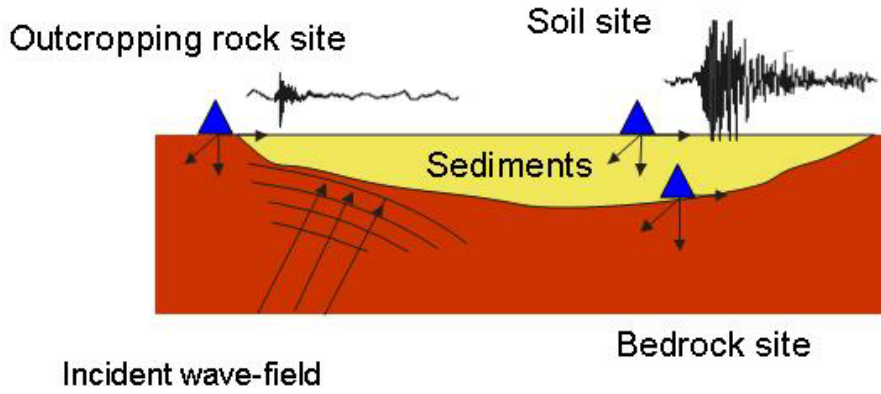
Fig. 14.3 Schematic description of the Reference Site Method. Blue triangles represent hypothetical seismological stations recording three component ground motion (directions are schematically indicated by the arrows).

14.2.1.1 Standard Spectral Ratio method (SSR)

The Standard Spectral Ratio technique (SSR) consists of comparing records at nearby sites, using one as the reference site (Figure 14. 3). It is assumed that records from the reference site (in general a station installed on outcropping hard bedrock) contain the same source and propagation effects as records from the other sites that is:

$$\frac{U_{ij}(f,r)}{U_{ik}(f,r)} = \frac{S_i(f)Z(f)_j A_{ij}(f,r)}{S_i(f)Z(f)_k A_{ik}(f,r)} \tag{14.2}$$

where, $U_{ij}(f,r)$ is the spectral amplitude of the ground motion observed at a recording site j for an event i, $S_i(f)$ is the source function, $Z_j(f)$ is the site response, $A_{ij}(f,r)$ is a function accounting for attenuation that includes the effect of geometrical spreading, intrinsic and scattering quality factor. f is the frequency, r the hypocentral distance and k indicates the reference station. Note, that similarly to what is schematically indicated in Figure 14.1, the ground motion recorded at one station is considered as the convolution of three terms, specifically the source $S_i(f)$, the path $A_{ij}(f,r)$ and site response $Z_j(f)$. If the stations are nearby and the reference station is not affected by site effects, then $Z_k = 1$ and $A_{ij}(f,r) \approx A_{ik}(f,r)$. Thus, the spectral ratio directly provides the site response at the non-reference stations. The major drawback of this method is that rock stations may also have their own response. Furthermore, a good reference site might be located too faraway from the target site therefore not allowing assuming similarity in the wave paths towards the two stations.

14.2.1.2 Generalized inversion technique (GIT)

The natural logarithm of the spectral amplitude $U_{ij}(f,r)$, observed at a recording site j for an event i, can be represented by:

$$\ln U_{ij}(f,r) = \ln S_i(f) + \ln Z(f)_j + \ln A_{ij}(f,r), \tag{14.3}$$

where, according to equation (14.2), $S_i(f)$ is the source function, $Z_j(f)$ is the site response, $A_{ij}(f,r)$ is a function accounting for attenuation, f is the frequency and r the hypocentral distance.

For all events and stations, equation (14.3) describes a linear system of the form $Ax = b$, which can be solved by using suitable inversion algorithms. The inversion can even be performed in two steps following the procedure of Castro et al. (1990). In the first step, the inversion is carried out to separate the source and attenuation effects without introducing any parametric model to describe the attenuation term $A_{ij}(f,r)$. The trade-off between attenuation and source is resolved by requiring that attenuation assumes an a priori chosen value at a given distance, irrespective of frequency. This assumption is justified by the small effect that the total attenuation (intrinsic and scattering) has on the decay of the wavefield amplitude at short distances. In the second step the inversion is carried out for the source and site functions, using the observed data that have been corrected for the attenuation. The undetermined degree of freedom of the second inversion is resolved by constraining the logarithm of the site amplification of the reference station (generally a rock site) to 0, irrespective of frequency. In cases when a reference site cannot be identified (for example by a simple horizontal-to-vertical spectral ratio of earthquake data; see next section 14.2.2) the average response of the whole network is constrained to 0. Although this restriction affects the absolute value of the single site functions, it does not affect the source functions.

Parolai et al., (2000) applied the GIT technique to investigate the site response at stations of a small urban network, while Bindi et al., (2009) used the GIT for estimating 2-D or 3-D site effects in a small basin. Recent examples of application of the GIT approach include Moya and Irikura (2003), who performed the inversion using a reference event instead of a reference site, Oth et al. (2008 and 2009), who applied the technique to an area where a simple parameterization of attenuation was not possible, and Drouet et al., (2008), who introduced a non-linear inversion scheme, although this is valid only under assumptions made on the source spectral shape.

14.2.2 Non-reference site techniques: H/V spectral ratio of earthquake data (EHV)

Non-reference site techniques allow to avoid the requirement of having a good hard rock reference station, either by making the assumption that the vertical component of the ground motion is not affected by amplification and that it is similar to the horizontal component at the bedrock (when earthquake recordings are used), or using seismic noise recordings generally dominated by surface waves (Fig. 14.4). While the assumption of the former cannot be true for frequencies higher than the fundamental one (Parolai and Richwalski, 2004), the second suffers from the lack of correlation between the estimated amplification level and that measured by earthquake data analysis. However, both methods can satisfactorily estimate the fundamental resonance frequency of a site.
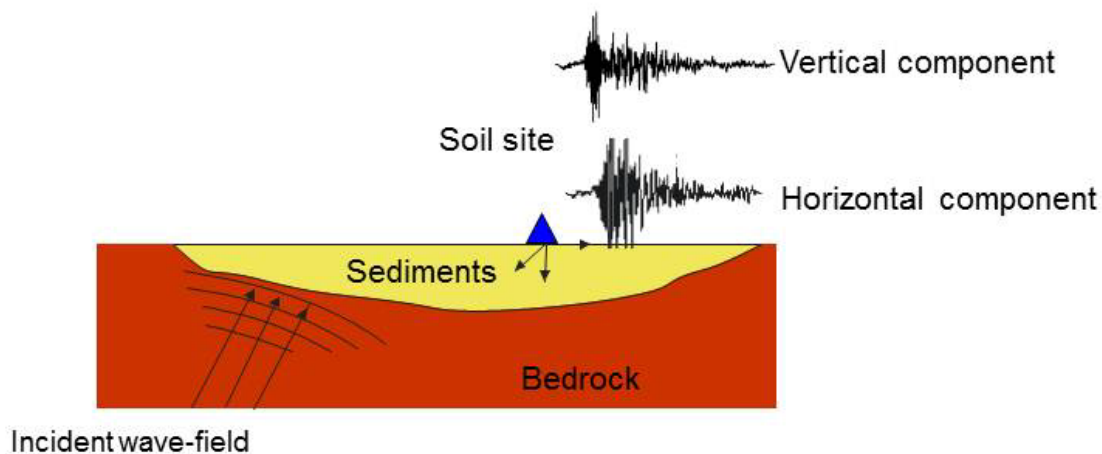
Fig. 14.4 Schematic description of the EHV method. The blue triangle represents a hypothetical seismological station recording three-component ground motion (directions are schematically indicated by the arrows). One horizontal component and the vertical component recordings are shown.

The EHV spectral ratio technique was introduced by Langston (1979) as a method to determine crustal and upper-mantle structure from teleseismic recordings. The basic assumption of the method is that the vertical component of motion is not influenced by the local structure, whereas the horizontal components contain the P-to-S conversions due to the geology underlying the station. Therefore, by deconvolving the vertical component from the horizontal, one could estimate the site response. The deconvolution is generally carried out by dividing the Fourier spectra of the horizontal component by the vertical one. However, the deconvolution operation is applied to data corrupted by noise and therefore, since this problem is ill-conditioned, small errors in the data could lead to solutions unacceptable from a physical point of view. Several regularization techniques are available to avoid artifacts in the results. The most common practice, although it is not properly a regularization approach, is to carry out the spectral ratio after having smoothed the spectra. The technique has been applied in many studies (e.g., Lermo and Chavez-Garcia, 1993; Field and Jacob, 1995; Lachet et al., 1996; Bonilla et al., 1997; Parolai et al., 2004; Parolai and Richwalski, 2004). In general, it was found that H/V ratios for S waves reveal the overall frequency dependence of the site response, even if the level of amplification, especially at frequencies higher than the fundamental one, can be different from that obtained by SSR analysis.

14.2.3 Vertical array data analysis

The increasing number of observations over the last few decades has greatly contributed towards the understanding of strong-motion site effects by the engineering and seismological communities, leading to advancements in the state of knowledge and modelling of in situ sediment response (Field et al., 1997). Nonetheless, finer resolution and more effective representation of the involved physics in the near surface medium require a good estimate of the input motion and of wave propagation in shallow layers. For this, by far, the best source of information is provided by downhole arrays, consisting of accelerometers recording ground motion at different depths and on the surface of the same site (see Chapter 7, Sub-chapter 7.4.6 on borehole strong-motion array installations).

Downhole measurements are a valuable complement to in situ and laboratory geotechnical investigation techniques. Indeed, they provide critical constraints for both the interpretation methods for surface observations as well as information on the real material behaviour and overall site response over a wide range of loading conditions (Assimaki et al., 2008). The amount and quality of information from downhole arrays in seismically active areas is the key for improving our understanding of in situ soil behaviour, assessing the modelling and parametric uncertainties associated with employed methodologies for strong-motion site-response analysis, and for shallow geological investigations.

Several methods have been proposed for estimating wave propagation velocity and damping from boreholes recordings. Amongst others, Trampert et al., (1993), van Vossen et al., (2004) and van Vossen et al., (2005), focused their attention on the SH phase propagation, while Mehta et al. (2007a; 2007b), starting from the similarity between deconvolution and the cross correlation tool used in seismic interferometry (e.g., Lobkins and Weaver 2001; Schuster et al., 2004; Shapiro and Campillo 2004; Snieder et al., 2006; Halliday and Curtis, 2008a), showed that the deconvolution of waveforms recorded by a vertical array can provide useful insight into the wavefield propagation in the uppermost crustal layers,. Although the use of the Fourier spectra amplitude ratio (uphole to downhole or with a reference station) is well known in engineering seismology (e.g., Safak, 1997), the deconvolution of seismograms (retaining information about phase) and their interpretation in the time domain has found few applications (Trampert et al., 1993; van Vossen et al., 2004; van Vossen et al., 2005). Assimaki et al.,(2008) proposed an inversion procedure that aims at estimating the best borehole model in term of shear wave velocity, attenuation and density, by optimizing the correlation between observed and synthetic seismograms. Parolai et al. (2009) showed by using a deconvolution approach that the wave propagation in the shallowest layer can be imaged independently on the chosen signal window and that down-going waves resulting from the reflection at the free surface might affect the recordings down to more than 100 m depth (see also Fig. 4.33 in Chapter 4). Yamada et al. (2010) estimated non-linear effects during strong shaking applying a deconvolution approach. Mogi et al., (2010) studied non-linear soil behaviour using a normalised input-output normalisation method. Parolai et al., (2010) showed that a robust estimate of an average Qs, that can be used for numerical simulations of ground motion, can be obtained by means of deconvolution of array recordings. Figure 14.5 shows an example of borehole recordings and of the relevant deconvolved wavefield.

It is worth noting how the ground motion is modified (in general amplified) with decreasing depth of recording, being largest at the surface. For this surface amplification effect see also Fig. 4.22 in Chapter 4 and Table 1 in EX 3.4. The deconvolved wavefield, obtained by analysing the signal window indicated in red in the left panel, clearly shows a peak in the a-causal (negative times) part of the signal propagating toward the surface with a velocity consistent with the S-wave velocity in the borehole (red dashed line). A peak corresponding to a downgoing wave is observed also at all the depths analyzed in the causal (positive times) part of the signal. But the downgoing wave peak has always smaller amplitude than the upgoing one due to the effect of attenuation.
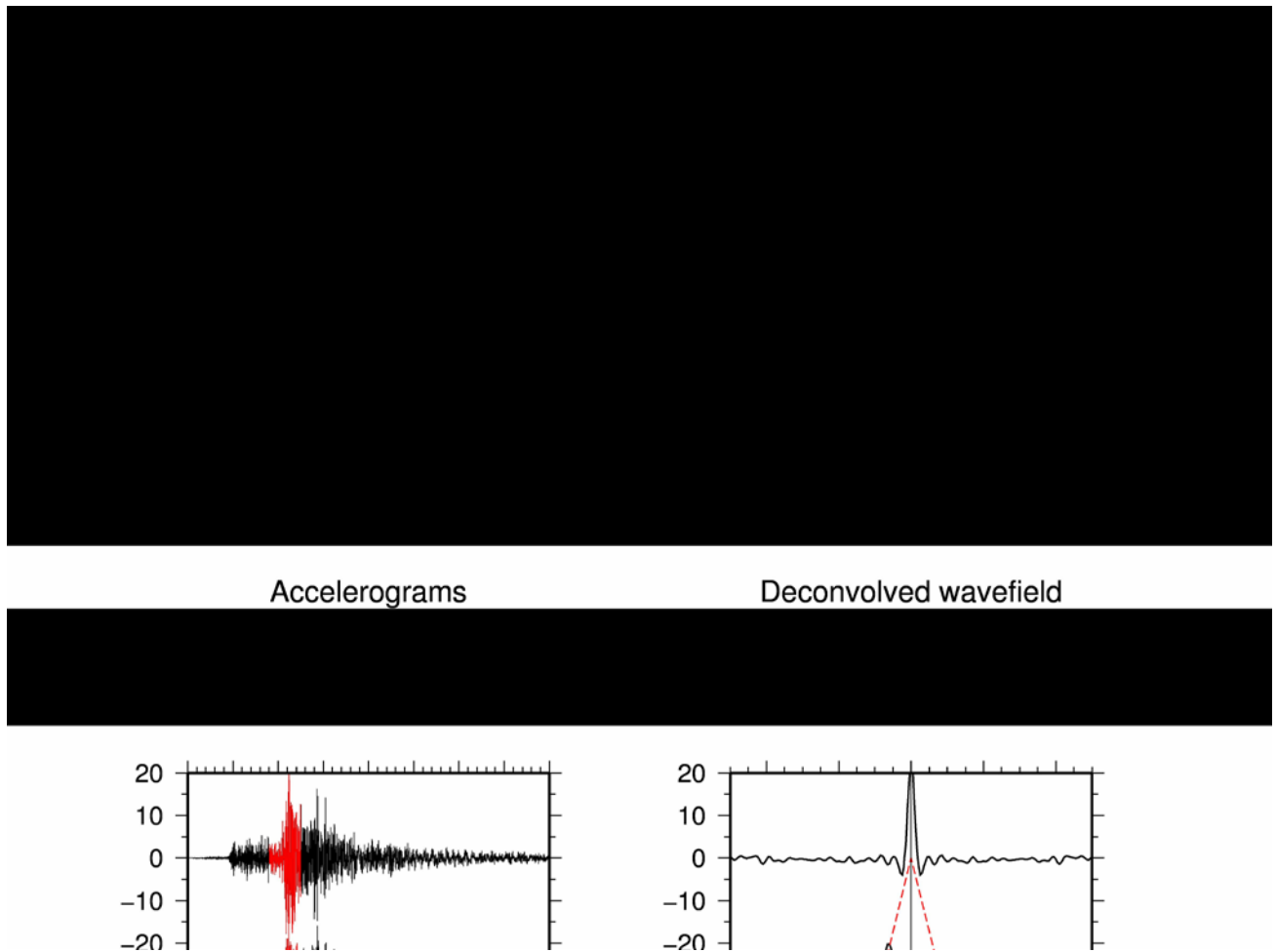

Fig. 14.5 Left-hand panel: horizontal component of ground acceleration recorded at different depths. Red record traces indicate the window containing S waves. **Right hand panel:** the upgoing (left) and downgoing (right) S waves in the deconvolved wavefield. The S-wave traveltimes, computed from the velocity model derived with the Parolai et al. (2005) inversion scheme, are indicated by the broken red lines.

14.3 Seismic noise measurements

14.3.1 Seismic Noise Horizontal-to-Vertical spectral ratio (NHV)

Nakamura (1989) revised the Horizontal-to-Vertical (H/V) seismic noise spectral ratio technique (NHV), first proposed by Nogoshi and Igarashi (1970 and 1971). Since then, in the field of site effect estimation, a large number of studies have been published, which use this

low cost, fast and therefore attractive technique (e.g. Field and Jacob, 1993; Lermo and Chavez-Garcia, 1994; Mucciarelli, 1998; Bard, 1999; Parolai et al., 2001b).

While in the Nakamura interpretation the NHV spectral ratio is directly related to the S-wave site response, most of the seismological/engineering community, based on the results of recent studies, is more inclined to consider predominant the role of surface waves (see e.g. Bard, 1999).

Most of the researchers focused their attention on the comparison of noise H/V spectral ratio and earthquake site response and agreed that the H/V spectral ratio of seismic noise provides a fair estimate of the fundamental resonance frequency of a site (Fig. 14.6). However, attempts to provide standards for the analysis of seismic noise have only recently been carried out (Bard, 1999; SESAME, 2003; Picozzi et al., 2005a). When using the NHV technique particular attention must be paid to the used seismic instruments and sensors (Guiller et al., 2007; Strollo et al., 2008a and b). Resonance frequency maps for large urban areas were recently provided by Parolai et al. (2001b) (Cologne, Germany), Duval et al. (2001) (Caracas, Venezuela), Picozzi et al. (2008) (Istanbul, Turkey), Bonnefoy-Claudet et al. (2009), Pilz et al. (2009 and 2010) (Santiago de Chile, Chile), Parolai et al. (2010b) (Bishkek, Kyrgyzstan, Figure14.7), after validation with earthquake data.
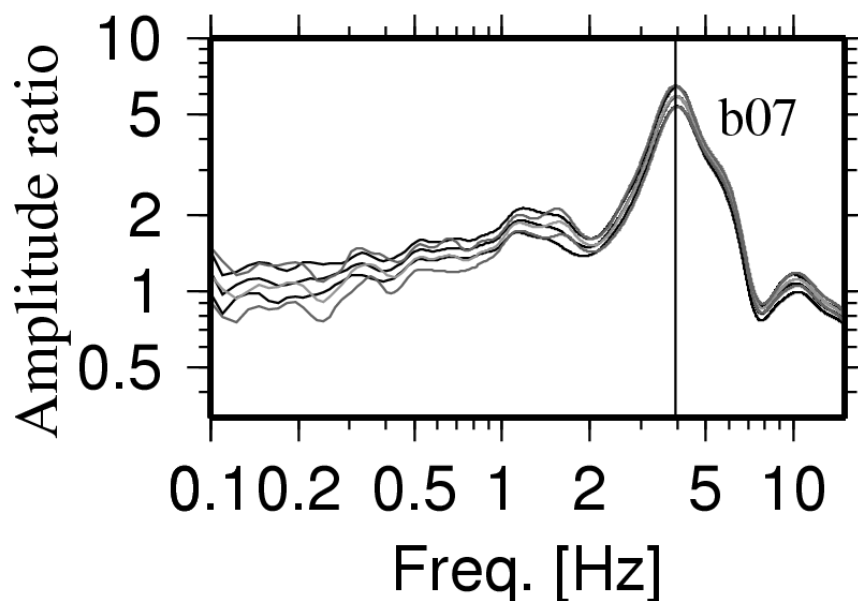

Fig. 14.6 Example of NHV ratio. The peak allows an estimate of the fundamental resonance frequency of the site (redrawn from Parolai and Galliana-Merino, 2006).
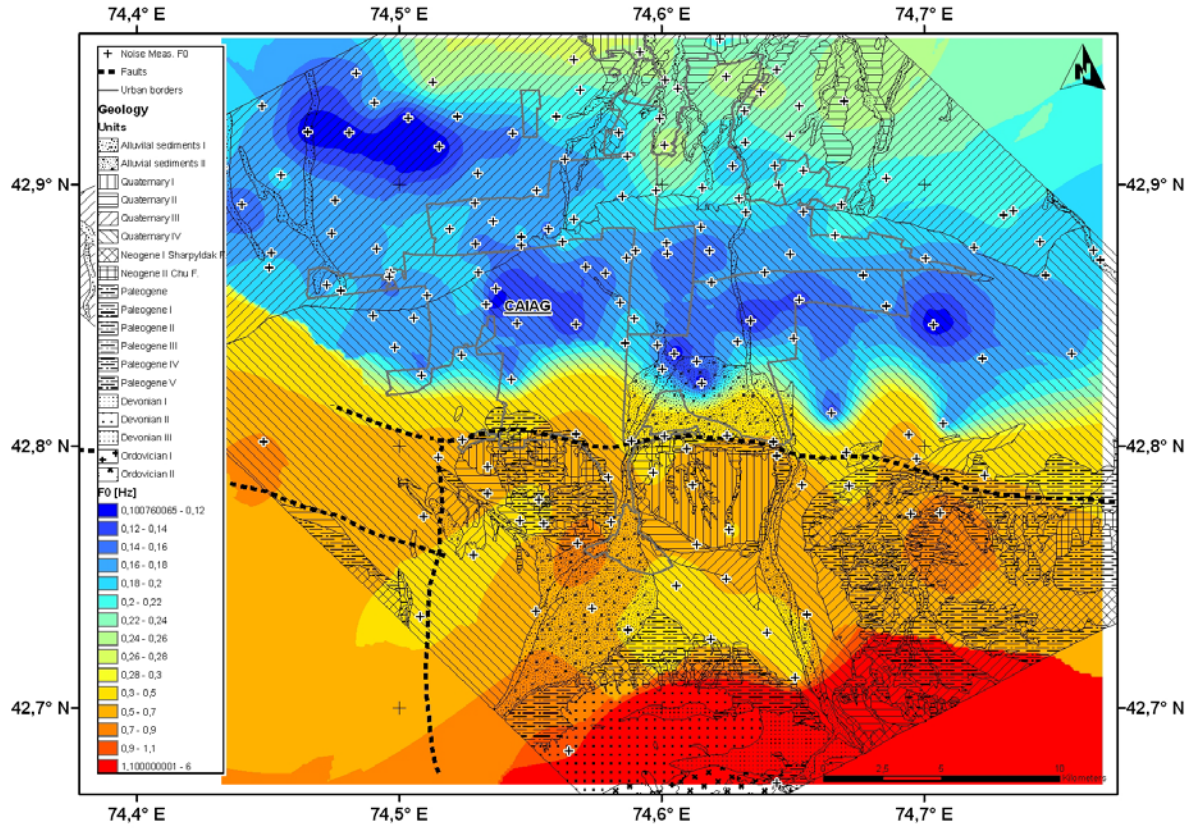
Fig. 14.7 Fundamental resonance frequency map of Bishkek (Kyrgyzstan). The crosses indicate sites where single station noise measurements were carried out. The map was obtained after interpolation between these points. A geological legend and sketch of the area is also shown.

14.3.1.1 Relationship between NHV peak frequency and thickness of the sedimentary cover

Recent studies (Yamanaka et al., 1994; Ibs-von Seht and Wohlenberg, 1999; Delgado et al., 2000 a and b; Parolai et al., 2002; D'Amico et al., 2008) showed that noise measurements can be used to map the thickness of soft sediments. Quantitative relationships between this thickness and the fundamental resonance frequency of the sedimentary cover as determined from the peak in the NHV spectral ratio were calculated for different basins in Europe (e.g. Ibs-von Seht and Wohlenberg, 1999; Delgado et al., 2000 a).

The approach is based on the assumption that in the investigated area, lateral variations of the S-wave velocity are minor and that it mainly increases with depth following a relation like

$$v_s(z) = v_{s0}(1 + Z)^x \tag{14.4}$$

where v_{s0} is the surface shear-wave velocity, $Z = z/z_0$ (with $z_0 = 1$ m) is the depth relative to z_0 and x describes the depth dependence of velocity. Taking this into account and considering the well-known relation among f_r (the resonance frequency), the average S-wave velocity of soft sediments $\overline{V_s}$, and the layer thickness h,

$$f_r = \overline{V_s}/4h, \tag{14.5}$$

the dependency between thickness and f_r can be written as

$$h = \left[v_{s0} \frac{(1-x)}{4 f_r} + 1 \right]^{1/(1-x)}$$

(14.6)

where f_r is to be given in Hz, v_{s0} in m/s and h in m. Moreover, empirical relationships between f_r and h in the form

$$h = a f_r^{\,b}$$

(14.7)

can also be derived, generally applying grid search procedures.

The above approximate interpretation can be easily extended to the case of a two layer sedimentary cover (D'Amico et al., 2008). Despite the fact that relatively large errors affect the depth estimates provided by this approach (D'Amico et al., 2004) it can be considered as a useful proxy for more costly exploratory surveys.

14.3.1.2 NHV inversion

Recently, the possibility of retrieving the S-wave velocity structure below a site from single station measurements based on NHV ratio computation was tested by Fäh et al. (2001). They suggested a new method for calculating NHV ratios employing a frequency-time analysis (FTAN). Moreover, after having shown that there is a good agreement between the NHV ratio and the theoretical ellipticity curves of the fundamental mode Rayleigh wave, they proposed to invert the NHV curve to derive directly the S-wave subsoil structure. The NHV was corrected for the contamination by SH and Love waves by simply reducing it by a factor $\sqrt{2}$, independent of frequency, under the assumption of an equal contribution to the seismic noise wavefield of Love and Rayleigh waves. The inversion, due to the non-linear nature of the problem, was based on a genetic algorithm (GA) (Fäh et al., 2001, 2003). The inversion is carried out for a fixed number of layers and a-priori defined ranges of the geophysical properties (S- and P-wave velocity, density and thickness) of the layers. An initial starting population of individuals is generated through a uniform distribution in the parameter space. The model that, amongst all those generated, allows the best reproduction of the observed NHV, is chosen as the best model.

Parolai et al. (2006) adopted this technique to derive S-wave velocity profiles in the Cologne area. Their inversions were carried out by fixing the total thickness of the sedimentary cover in order to avoid problems of trade-off between the total thickness and the S-wave velocity (Scherbaum et al., 2003; Arai and Tokimatsu, 2004). For each site, different inversions were carried out, varying the thickness of the sedimentary layer considering the uncertainty in its estimate. The best models obtained from each inversion were averaged.

In Parolai et al. (2006) the inversion of NHV curves was extended to 20 of the sites measured by Parolai et al. (2001b) and a 2-D S-wave velocity model was derived by means of interpolating between the derived 20 depth profiles. Figure 14.8 shows the resulting 2-D S-wave velocity model (bottom) together with the geological cross-section. The agreement between the geological structure obtained by interpretation of boreholes data and surface geology, and the S-wave velocity model is very good. Compared to the average velocity relationship previously derived for the whole area (Parolai et al., 2002; see also section 14.3.1.1), lateral variations in the velocity structure are clearly visible.
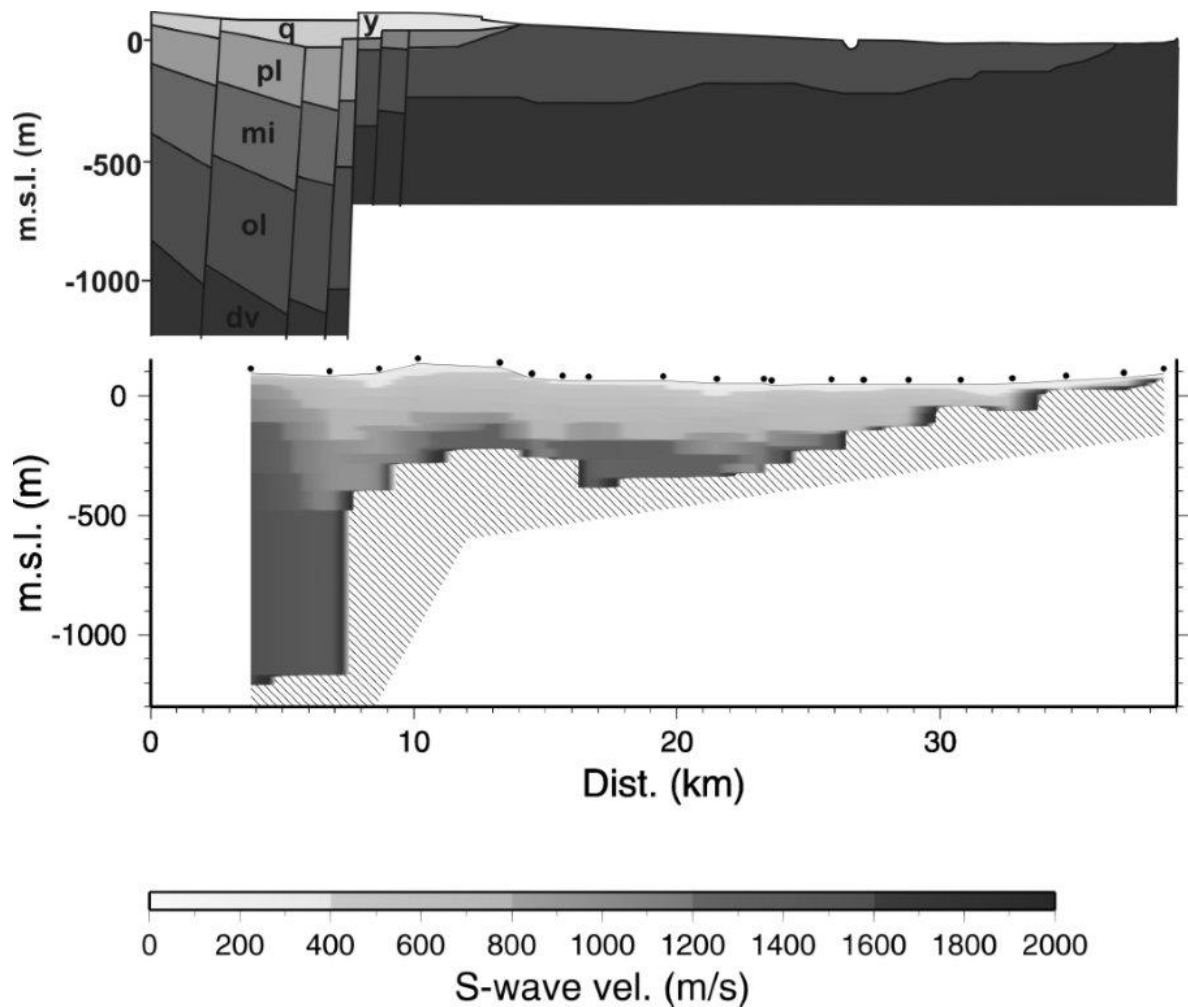
Fig. 14.8 Top: Geological cross section of the sedimentary cover in Cologne (redrawn after Von Kamp, 1986) y = Landfills, q = Quaternary, pl = Pliocene, mi = Miocene, ol = Oligocene, dv = Devonian. Bottom: 2-D S-wave velocity model interpolated from 1-D S-wave velocity profiles calculated for 20 selected sites where the NHV was inverted. The striped pattern indicates the Devonian bedrock inverted (modified after Parolai et al., 2006).

Therefore, in this case of well constrained bedrock depth, it could be shown that the sedimentary cover is fairly regularly layered, and the NHV inversion a suitable method for quickly mapping 3-D S-wave velocity structures. The vertical resolution of the profiles was also found sufficient to provide site responses (Parolai et al., 2006; Parolai et al., 2007) by means of numerical simulations, in agreement with the empirical ones.

Recently, improvement in the forward calculation of NHV spectral ratios were proposed by Arai and Tokimatsu (2000, 2004) and applied in a joint inversion scheme of NHV and dispersion curves by Parolai et al. (2005), Picozzi and Albarello (2007) and D'Amico et al. (2008).

Arai and Tokimatsu (2000) showed that NHV spectral ratios can be better reproduced if the contribution of higher modes of Rayleigh waves and Love waves is also taken into account. They suggest to calculate the NHV spectral ratio as

$$\left(NHV \right)_{s} = (P_{HS}/P_{VS})^{1/2} \tag{14.8}$$

where the sub-index s stands for surface waves, and P_{VS} and P_{HS} are the vertical and horizontal powers of surface waves (Rayleigh and Love), respectively.

The vertical power of the surface waves is only determined by the vertical power of Rayleigh waves (P_{Vr}), while the horizontal power involves the contribution of both Rayleigh (P_{HR}) and Love waves (P_{HL}). The following equations can therefore be used (Harkrider, 1964):

$$P_{VS} = P_{VR} = \sum_{j} \left(A_{Rj}/k_{Rj} \right)^{2} \left\{ 1 + \left(\alpha^{2}/2 \right)\left(u/w \right)_{j}^{2} \right\} \tag{14.9}$$

$$P_{HS} = P_{HR} + P_{HL} \tag{14.10}$$

$$P_{HR} = \sum_{j} \left(A_{Rj}/k_{Rj} \right)^{2} \left(u/w \right)_{j}^{2} \left\{ 1 + \left(\alpha^{2}/2 \right)\left(u/w \right)_{j}^{2} \right\} \tag{14.11}$$

$$P_{HL} = \sum_{j} \left(A_{Lj}/k_{Lj} \right)^{2} \left(\alpha^{2}/2 \right) \tag{14.12}$$

where A is the medium response, k is the wavenumber, u/w is the H/V ratio of the Rayleigh mode at the free surface, j is the mode index, and α is the H/V ratio of the loading horizontal and vertical forces L_H/L_V.

Picozzi et al. (2005b) showed that varying α over a large range did not significantly changed the NHV shape. Therefore, they used $\alpha=1$.

A basic problem of these inversion procedures concerns the choice of the frequency band to be used for the inversion of the NHV curve. As an example, the NHV values around the maximum have been discarded by Parolai et al. (2006) since the effect of smoothing of the spectra biases the amplitude estimation around this frequency band. Instead, they have been taken into account by Picozzi and Albarello (2007) and D'Amico et al., (2008), who tried to exploit the effect of higher modes around the fundamental resonance frequency value. Recent theoretical studies (Lunedei and Albarello, 2009; Albarello and Lunedei, 2009) indicate that the NHV curve around the fundamental resonance frequency f_0 (i.e., around the NHV maximum) can be significantly affected by the damping profile in the subsoil and by the distribution of sources around the receiver. In particular, they showed that sources located within few hundreds of meters from the receiver can generate seismic phases that strongly affect the shape of the NHV curve around and below f_0. This implies that, unless a large source-free area exists around the receiver, inversion of the NHV shape (around and below f_0) carried out by using forward models based on surface waves only, might provide biased results. However, these conclusions still need to be confirmed by comparison with real data.

Recently, Pilz et al. (2010) obtained a 3-D S-wave velocity model of the Santiago de Chile basin by inverting with this method the NHV ratio calculated in Pilz et al. (2009). In order to reduce the trade-off between thickness of the sedimentary cover and S-wave velocity they constrained the former to values derived by previously carried out gravimetric measurements. An example of the results is shown in Figure 14.9.
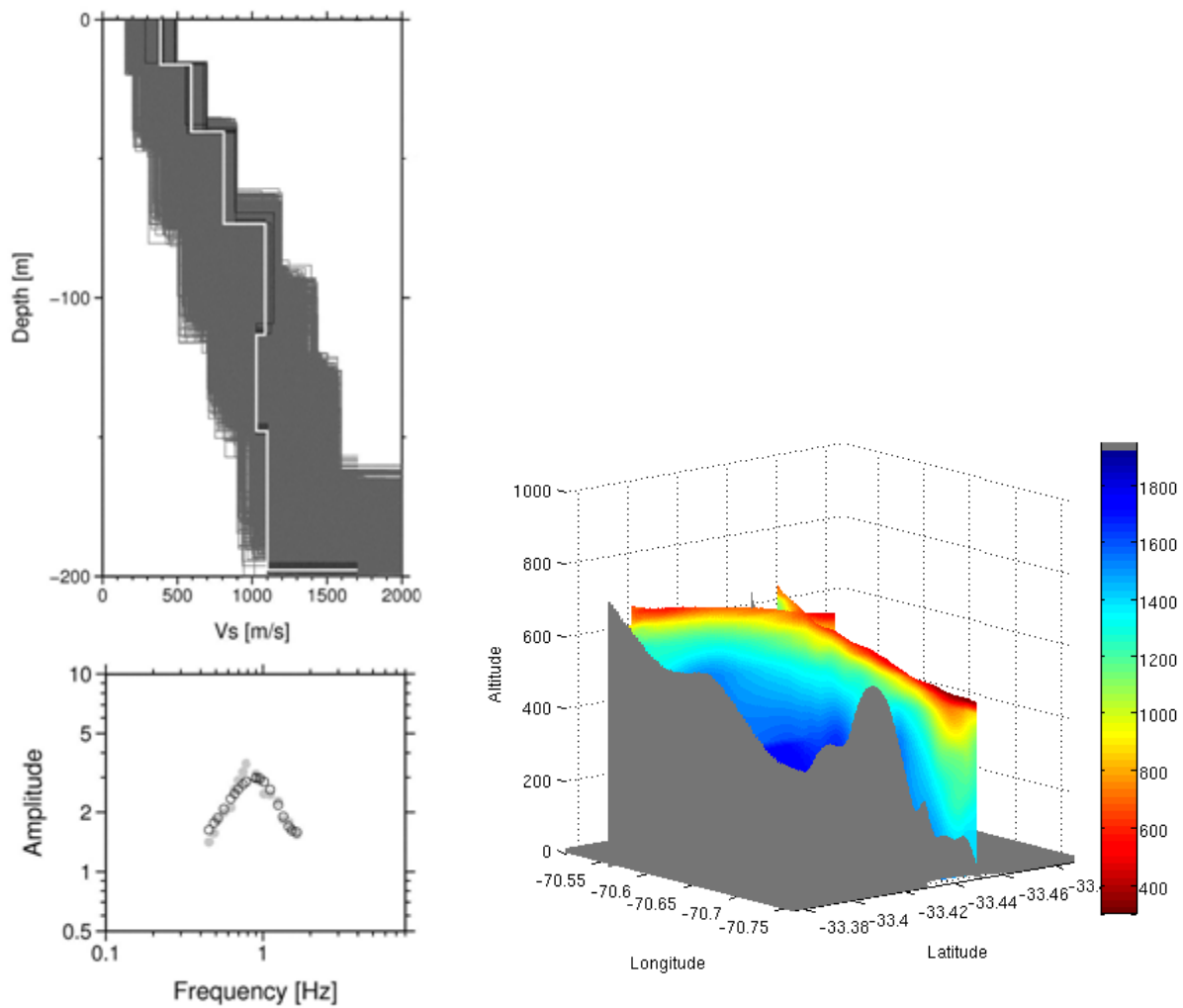
Figure 14.9 Left: Example of S-wave velocity profile derived by NHV inversion. The best model (white line), the models lying within the 10% of the minimum misfit (black lines) and all the tested models (gray lines) are shown. The bottom panel shows the observed (gray circles) and calculated (empty circles) for the best models NHV. **Right:** The 3-D model of the Santiago de Chile basin obtained by interpolating between the S-wave velocity-depth profiles like the one in the upper left corner of this figure. The color scale indicates the S-wave velocities in m/sec.

14.4 2-D arrays

Seismic arrays were originally proposed at the beginning of the 1960s as a new type of seismological tool for the detection and identification of nuclear explosion (e.g., Bormann, 1966; Frosch and Green, 1966). Since then, seismic arrays have been applied at various scales for many geophysical purposes. At the seismological scale, they were used to obtain refined velocity models of the Earth's interior (e.g., Birtill and Whiteway, 1965; Whiteway, 1966; Kværna, 1989; Kárason and van der Hilst, 2001; Ritter et al., 2001; Krüger et al., 2001). Reviews on array applications in seismology can be found in Chapter 9 of this Manual, in Douglas (2002) and in Rost and Thomas (2002). At smaller scales, since the pioneering work of Aki (1957), seismic arrays have been used for the characterization of surface wave

propagation, and the extraction of information on the shallow subsoil structure (i.e., the estimation of the local S-wave velocity profile). Especially in the last decades, due to the focus of seismologists and engineers on estimating the amplification of earthquake ground motion as a function of local geology, the improvements in the quality of instrumentation and computing power, interest in analyzing seismic noise recorded by arrays has grown (e.g., Horike, 1985; Hough et al., 1992; Ohori et al., 2002; Okada, 2003; Scherbaum et al. 2003; Parolai et al., 2005; Tada et al., 2006; Asten, 2006; Köhler et al., 2007). A review on array application for site classification can be found in Foti et al. (2011).

14.4.1 f-k based methods

The phase velocity of the surface waves can be extracted from noise recordings by using different methods. Here we will illustrate the two most frequently used methods for f-k (frequency-wavenumber) analysis: the Beam-Forming Method (BFM) (Lacoss et al., 1969) and the Maximum Likelihood Method (MLM) (Capon, 1969).

The estimate of the f-k spectra $P_b(f,k)$ by the BFM is given by:

$$P_b(f,k) = \sum_{l,m=1}^{n} \phi_{lm} \exp\{ik(X_l - X_m\} \ ,$$

(14.13)

where f is the frequency, k the two-dimensional horizontal wavenumber vector, n the number of sensors, ϕ_{lm} the estimate of the cross-power spectra between the lth and the mth recordings, and X_l and X_m, are the coordinates of the lth and m[th] sensors, respectively.

The MLM gives the estimate of the f-k spectra $P_m(f,k)$ as:

$$P_m(f,k) = \left(\sum_{l,m=1}^{n} \phi_{lm}^{-1} \exp\{ik(X_l - X_m\} \right)^{-1} .$$

(14.14)

Capon (1969) showed that the resolving power of the MLM is higher than that of the BFM, however, the MLM is more sensitive to measurement errors.

From the peak in the f-k spectrum occurring at coordinates k_{xo} and k_{yo} for a certain frequency f_0, the phase velocity c_0 can be calculated by:

$$c_0 = \frac{2\pi f_0}{\sqrt{k_{xo}^2 + k_{yo}^2}} \quad .$$

(14.15)

An extensive description of these methods can be found in Horike (1985) and Okada (2003).

The estimate EP_b and EP_m of the true P_b and P_m f-k spectra may be considered in the convolution of the true functions with a frequency window function W_f and the wavenumber window functions W_B and W_M for the BFM and MLM, respectively (Lacoss *et al.*, 1969). The first window function W_f is the transfer function of the tapering function applied to the signal time windows (Kind, 2005). The function W_B is termed differently by various authors (e.g., "*spatial window function*" by Lacoss et al., 1969, and "*beam-forming array response function*" by Capon, 1969), and hereafter simply defined as Array Response Function (ARF). The ARF depends only on the distribution of stations in the array and has for the wavenumber vector k_o the form (Horike, 1985)

$$W_B(k, k_o) = \frac{1}{n^2} \sum_{l,m=1}^{n} \exp\{i(k - k_o)(X_l - X_m)\}. \tag{14.16}$$

Simply speaking, it represents a kind of spatial filter for the wavefield. The main advantage of the MLM with respect to the BFM involves the use of an improved wavenumber window W_M. Namely, for a wavenumber k_0 this window function may be expressed in the form

$$W_M(f, k, k_0) = \left| \sum_{j=1}^{N} A_j(f, k_0) \right| W_B(k, k_0), \tag{14.(17)}$$

where

$$A_j(f, k_0) = \frac{\sum_{l=1}^{N} q_{jl}(f, k_0)}{\sum_{j,l=1}^{N} q_{jl}(f, k_0)} \tag{14.18}$$

and q_{jl} represents the elements of the cross-power spectral matrix. It is evident that W_M depends not only on the array configuration, through the function W_B, but also on the quality (i.e., signal-to-noise ratio) of the data (Horike, 1985). In fact, the wavenumber response is modified by using the weights $A_j(f, k_0)$, which depend directly on the elements $q_{jl}(f)$. In practice, W_M allows the monochromatic plane wave travelling at a velocity corresponding to the wavenumber k_0 to pass undistorted, while it suppresses, in an optimum least-square sense, the power of those waves travelling with velocities corresponding to wavenumbers other than k_0 (Capon, 1969). Or, in other words, coherent signals are associated with large weights of A_j and their energy is emphasized in the f-k spectrum. On the contrary, if the coherency is low, the weights A_j are small and the energy in the f-k spectrum is damped (Kind et al., 2005). This automatic change of the main-lobe and side-lobe structure minimizes the leakage of power from the remote portion of the spectrum and has a direct positive effect on the P_m function, and consequently on the following velocity analysis. However, considering the dependence of W_M on W_B, it is clear that the array geometry is a factor which has a strong influence on both EP_b and EP_m. In fact, similarly to every kind of filter, several large side lobes located around the major central peak can remain in the f-k spectra (Okada, 2003) and cause serious biases in the velocity and back-azimuth estimates. In particular, side-lobe height and main-lobe width within W_B control the leakage of energy and resolution, respectively (Zywicki, 1999).

As a general criterion, the error in the velocity analysis due to the presence of spurious peaks in the f-k spectra may be reduced using distributions of sensors for which the array response approaches a two-dimensional δ-function. For that reason, it is considered a good practice to undertake a preliminary evaluation of the array response when the survey is planned. Irregular configurations of even only a few sensors should be preferred, because they allow one to obtain a good compromise between a large aperture, which is necessary for sharp main peaks in the EP_b and EP_m, and small inter-sensor distances, which are needed for large aliasing periods (Kind et al., 2005).

Recently, Picozzi et al. (2010a) showed that removing the effect of the array response from the frequency wavenumber images by using the Richards-Lucy regularization method improve the phase velocity estimation.

Fig.14.10 shows an example of 2-D-array configuration and its respective array responses. Figure 14.11 shows an example of f-k analysis results for 3.15 Hz, 5.6 Hz, and 9.9 Hz for the array configuration of Fig. 14.10. White dots indicate the position of the maximum used to estimate the phase velocity while the white circles join points with the same k values.
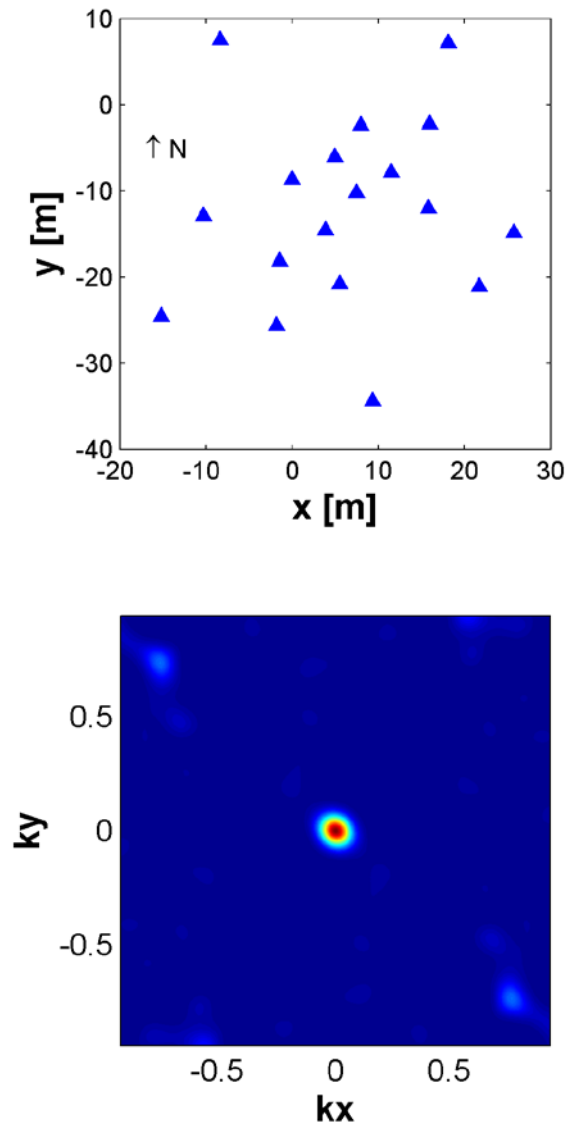

Fig. 14.10 Top: Example of a micro-array configuration. The blue triangles indicate the station positions. **Bottom:** The relevant micro-array response estimated for the frequency of 15 Hz.
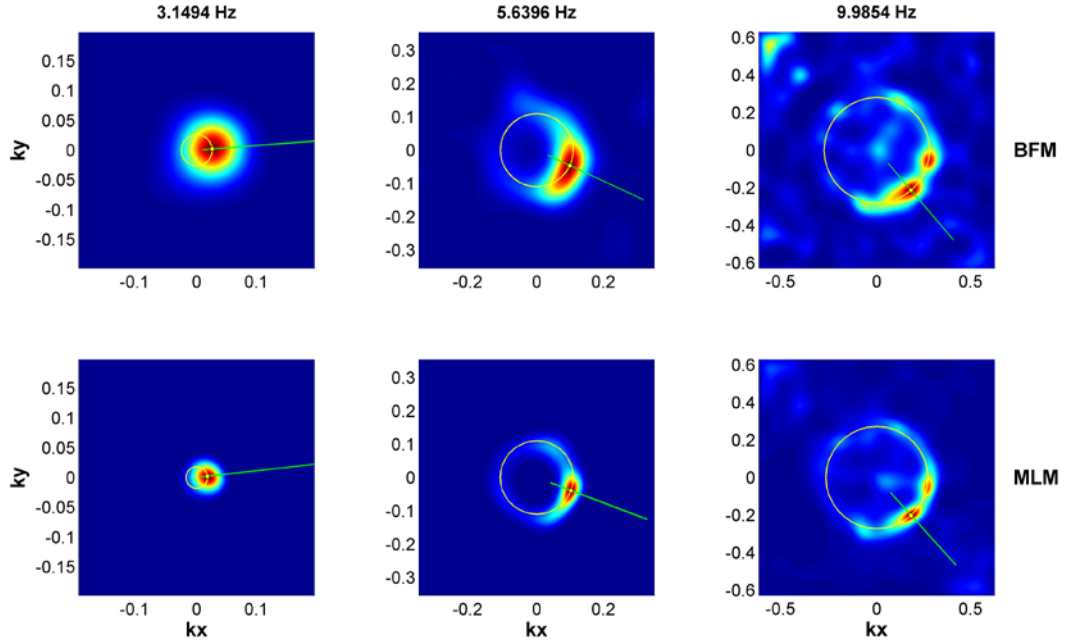
Fig. 14.11 Example of results from f-k analysis for 3.15 Hz, 5.6 Hz, and 9.9 Hz. White dots indicate the position of the maximum used to estimate the phase velocity. The circles join points with the same k. In this case at frequencies of 5.6 and 9.9 Hz the velocity of propagation of waves can be estimated and the source position identified (red color in the maps). (Comment: There are as many white dots as circles. Thus both has to be plural)

14.4.2 Spatial and Extended Spatial Autocorrelation method (SPAC and ESAC)

Aki (1957 and 1965) showed that phase velocities in sedimentary layers can be determined using a statistical analysis of ambient noise. He assumed that noise represents the sum of plane waves propagating without attenuation in a horizontal plane in different directions with different powers, but with the same phase velocity for a given frequency. He also assumed that waves with different propagation directions and different frequencies are statistically independent. Then, a spatial correlation function can be defined as

$$\phi(r, \lambda) = < u(x, y, t)(x + r\cos(\lambda), y + r\sin(\lambda), t) > \qquad (14.19)$$

where $u(x, y, t)$ is the velocity observed at point (x,y) at time t; r is the inter-station distance; λ is the azimuth and $< >$ denotes the ensemble average. An azimuthal average of this function is given by

$$\phi(r) = \frac{1}{\pi} \int_0^\pi \phi(r, \lambda) d\lambda. \qquad (14.20)$$

For the vertical component, the power spectrum $\phi(\omega)$ can be related to $\phi(r)$ via the zero[th] order Hankel transform:

20

$$\phi(r) = \frac{1}{\pi} \int_0^\infty \phi(\omega) J_0\left(\frac{\omega}{c(\omega)} r\right) d\omega, \tag{14.21}$$

where ω is the angular frequency, $c(\omega)$ is the frequency-dependent phase velocity, and J_0 is the zero order Bessel function. The space-correlation function for one angular frequency ω_0, normalized to the power spectrum, will be of the form

$$\phi(r, \omega_o) = J_0\left(\frac{\omega_0}{c(\omega_0)} r\right). \tag{14.22}$$

By fitting the azimuthally averaged spatial correlation function obtained from measured data to the Bessel function, the phase velocity $c(\omega_0)$ can be calculated. A fixed value of r is used in the spatial autocorrelation method (SPAC). However, Okada (2003) and Ohori et al. (2002) showed that, since $c(\omega)$ is a function of frequency, better results are achieved by fitting the spatial-correlation function at each frequency to a Bessel function, which depends on the inter-station distances (extended spatial autocorrelation, ESAC). For every couple of stations the function $\phi(\omega)$ can be calculated in the frequency domain by means of (Malagnini et al., 1993; Ohori et al., 2002; Okada, 2003):

$$\phi(\omega) = \frac{\frac{1}{M} \sum_{m=1}^M \mathrm{Re}\left({}_m S_{jn}(\omega)\right)}{\sqrt{\frac{1}{M} \sum_{m=1}^M {}_m S_{jj}(\omega) \sum_{m=1}^M {}_m S_{nn}(\omega)}}, \tag{14.23}$$

where ${}_m S_{jn}$ is the cross-spectrum for the mth segment of data, between the jth and the nth station; M is the total number of used segments. The power spectra of the mth segments at station j and station n are ${}_m S_{jj}$ and ${}_m S_{nn}$, respectively.

The space-correlation values for every frequency are plotted as a function of distance, and an iterative grid-search procedure can then be performed using equation (14.22) in order to find the value of $c(\omega_0)$ that gives the best fit to the data. The tentative phase velocity $c(\omega_0)$ is generally varied over large intervals (e.g., between 100 and 3000 m/s) in small steps (e.g., 1 m/s). The best fit is achieved by minimizing the root mean square (RMS) of the differences between the values calculated with equation (14.21) and (14.22). Data points, differing more than two standard deviations from the value obtained with the minimum-misfit velocity, can be removed before the next iteration of the grid-search. Parolai et al. (2006) used this procedure and allowed for a maximum of three grid-search iterations. An example of the application of this procedure is shown Fig. 14.12.

Several studies, (e.g. Parolai et al., 2009, Foti et al., 2011) showed the reliability of the procedure in deriving a robust estimate of the dispersion curve that lead to S-wave velocity profiles consistent with those obtained by other geophysical methods.
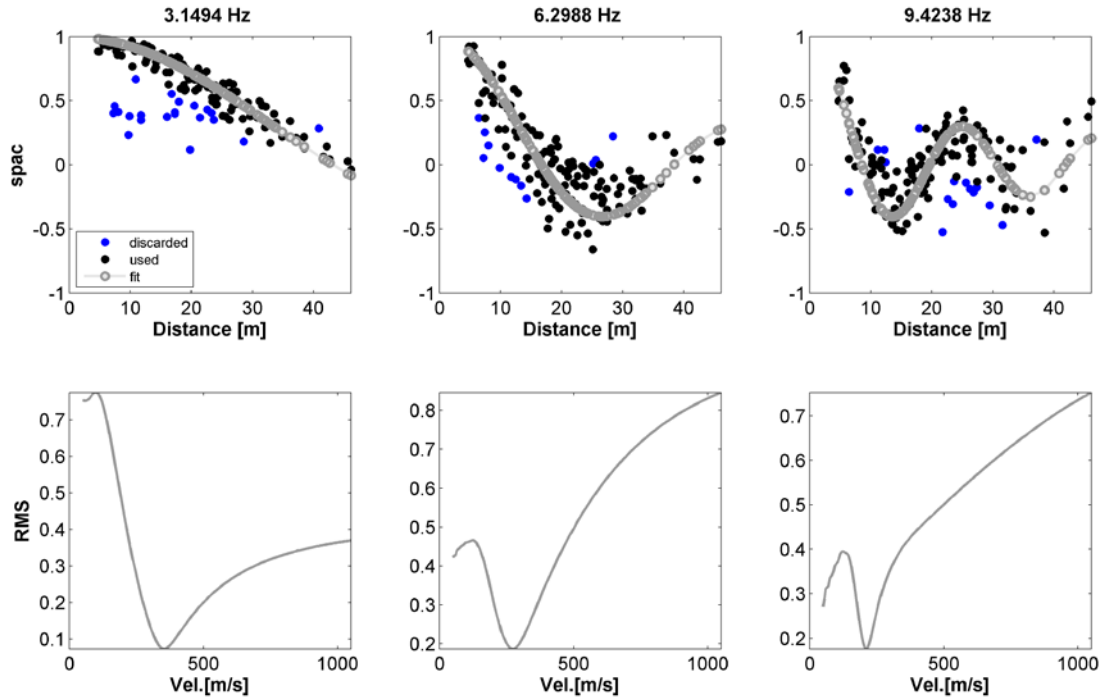
Fig. 14.12 Top: Measured space-correlation function values for different frequencies (black and blue circles) and the best-fitting Bessel function (gray circles). Discarded values (blue circles) lie two standard deviations outside the curve. **Bottom:** The respective RMS error versus phase velocity curves.

The ESAC method can be adopted to derive the phase velocities for all frequencies composing the Fourier spectrum of the data. Figure 14.12 shows on top three examples of the space-correlation values computed from the data together with the best fitting Bessel functions and below the corresponding RMS errors as function of the tested phase velocities, exhibiting clear minima. For high frequencies, the absolute minimum might sometimes corresponds to the minimum velocity chosen for the grid search procedure. This solution is then discarded, because a smooth variation of the velocity between close frequencies is required. At frequencies higher than a certain threshold the phase velocity might increase linearly. This effect is due to spatial aliasing which limits the upper bound of the usable frequency band. It depends on the S-wave velocity structure at the site and the minimum inter-station distance. At low frequencies the RMS error function clearly indicates the lower boundary for acceptable phase velocities, but might not be able to constrain the higher ones (then a plateau can appear in the RMS curves). The frequency above which phase differences cannot be resolved any more depends on the maximum inter-station distance and the S-wave velocity structure below the site: a wide range of velocities will then explain the observed small phase differences. Zhang et al. (2004) clearly pointed out this problem in Equation (3a) of their article.

Figure 14.13 gives an example of the final dispersion curve. The typical behaviour of f-k methods, namely of BFM to yield higher phase velocities than the ESAC method at low frequencies (Okada 2003), is clearly to be seen. Yet, Okada (2003) showed that by increasing the array size, the f-k velocities at low frequencies become similar to those estimated by ESAC, indicating that the latter is more suitable for providing reliable dispersion curves over

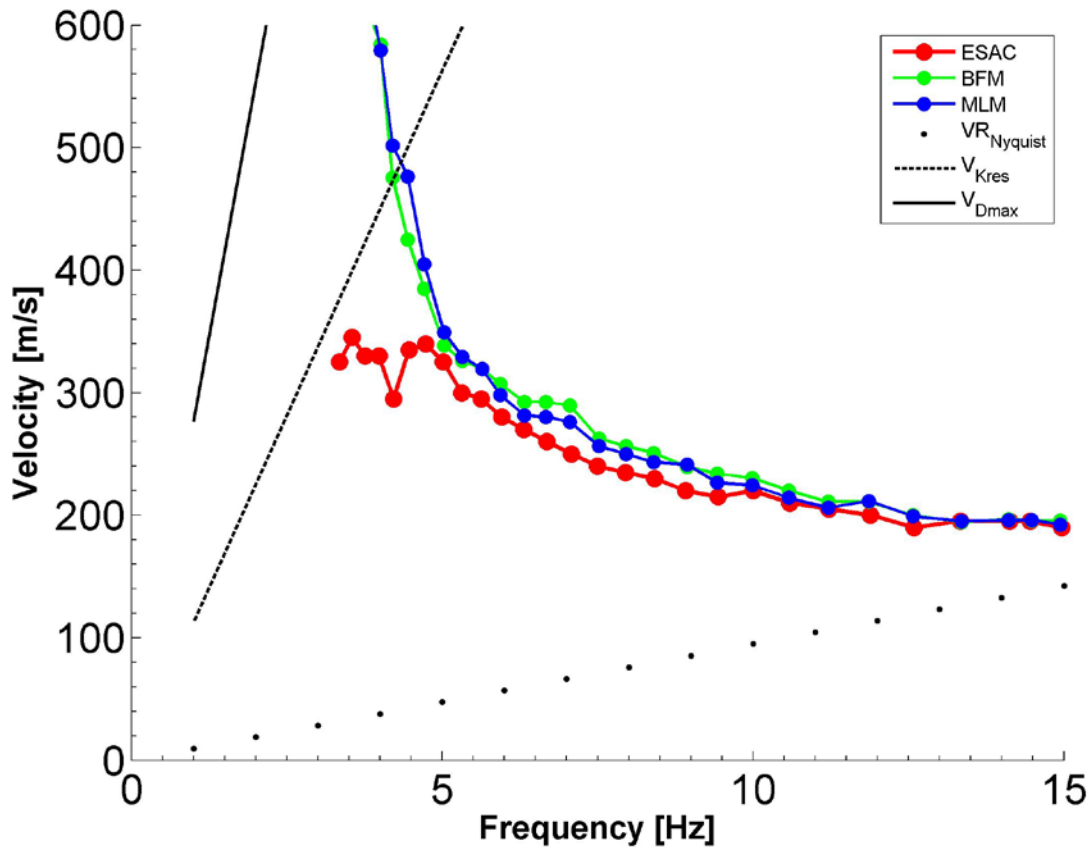a wider frequency range, especially toward lower frequencies (and thus with greater penetration depths).

Fig. 14.13 Phase velocity dispersion curves obtained by ESAC (reds line), BFM (green line) and MLM (blue line) analysis. The dotted line indicate the theoretical aliasing limit calculated as $4f$ dmin, where dmin is the minimum interstation distance. The factor 4 is used instead of the generally used factor 2, because the minimum distance in the array is appearing only once. The dashed gray line indicates the lower frequency threshold of the analysis based on $2\pi f \Delta k$ where Δk is calculated as the half-width of the main peak in the array response function. The continuous line indicates the lower frequency threshold of the analysis based on the equation $3f$ dmax, where dmax is the maximum interstation distance in the array

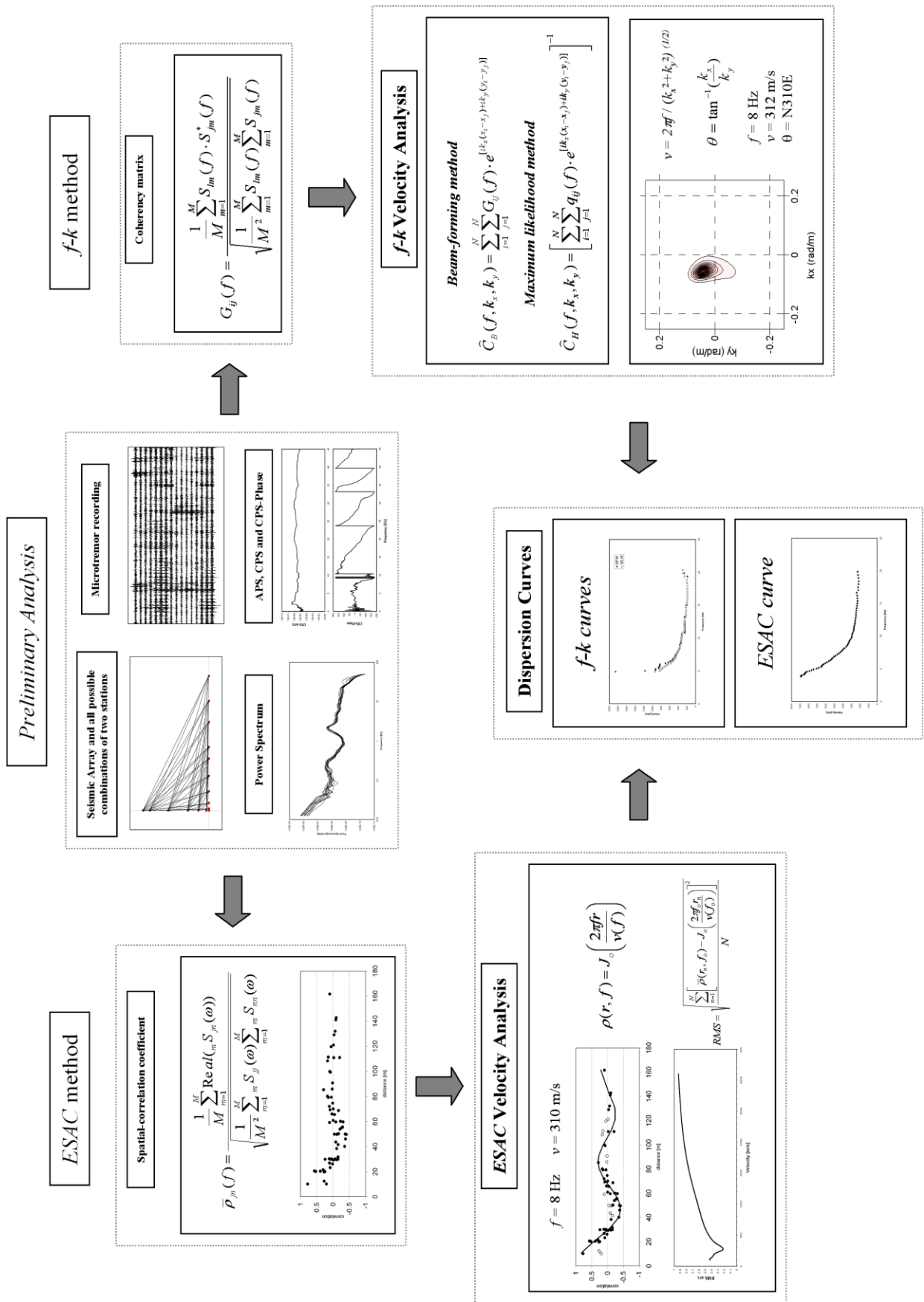Figure 14.14 summarises the procedure used with the ESAC and f-k methods.

f-k method

Coherency matrix

$$G_{ij}(f) = \frac{\frac{1}{M}\sum_{m=1}^{M} S_{im}(f)\cdot S_{jm}^{*}(f)}{\sqrt{\frac{1}{M^{2}}\sum_{m=1}^{M}S_{im}(f)\sum_{m=1}^{M}S_{jm}(f)}}$$

Preliminary Analysis

Microtremor recording

APS, CPS and CPS-Phase

Seismic Array and all possible combinations of two stations

Power Spectrum

f-k Velocity Analysis

Beam-forming method

$$\hat{C}_{B}(f,k_{x},k_{y}) = \sum_{i=1}^{N}\sum_{j=1}^{N} G_{ij}(f)\cdot e^{[k_{x}(x_{i}-x_{j})+ik_{y}(y_{i}-y_{j})]}$$

Maximum likelihood method

$$\hat{C}_{H}(f,k_{x},k_{y}) = \left[\sum_{i=1}^{N}\sum_{j=1}^{N} q_{ij}(f)\cdot e^{[ik_{x}(x_{i}-x_{j})+ik_{y}(y_{i}-y_{j})]}\right]^{-1}$$

$$v = 2\pi f / (k_{x}^{2}+k_{y}^{2})^{(1/2)}$$

$$\theta = \tan^{-1}\left(\frac{k_{x}}{k_{y}}\right)$$

$f = 8$ Hz
$v = 312$ m/s
$\theta = $ N310E

ky (rad/m)
kx (rad/m)

Dispersion Curves

f-k curves

ESAC curve

ESAC method

Spatial-correlation coefficient

$$\bar{\rho}_{jn}(f) = \frac{\frac{1}{M}\sum_{m=1}^{M}\mathrm{Real}(S_{jn}(\omega))}{\sqrt{\frac{1}{M^{2}}\sum_{m=1}^{M}S_{jj}(\omega)\sum_{m}S_{nn}(\omega)}}$$

correlation
distance [m]

ESAC Velocity Analysis

$f = 8$ Hz $v = 310$ m/s

$$\rho(r,f) = J_{o}\left(\frac{2\pi f r}{v(f)}\right)$$

$$RMS = \sqrt{\frac{\sum_{n=1}^{N}\left[\bar{\rho}(r_{n},f_{o}) - J_{o}\left(\frac{2\pi f r_{n}}{v(f_{o})}\right)\right]^{2}}{N}}$$

correlation
distance [m]

Fig. 14.14 Summary of the procedure used with the ESAC and f-k methods (from Picozzi, 2006)

14.5 Interferometry and tomography

Recent theoretical studies have shown that the cross-correlation of diffuse wavefields can provide an estimate of the Green's functions between receivers (Weaver and Lobkis, 2001 and 2004; Snieder, 2004; Wapenaar, 2004; Wapenaar and Fokkema, 2006). Using coda waves of seismic events (Campillo and Paul, 2003) and long seismic noise sequences (Shapiro and Campillo, 2004), it was confirmed that it is possible to estimate the Rayleigh wave component of Green's functions between two stations by the cross-correlation of simultaneous recordings. This method is now generally referred to as seismic interferometry. These results allowed the first attempts of surface wave tomography at regional scales (e.g., Shapiro and Campillo, 2004; Sabra et al., 2005; Shapiro et al., 2005; Gerstoft et al., 2006; Yao et al., 2006; Cho et al., 2007; Lin et al., 2007; Yang et al., 2007) using seismic noise recordings from broad-band seismic networks. Generally, for these kinds of studies, waves at frequencies well below 1 Hz were used to image the crust and the upper-mantle structure. A comprehensive review of the seismic interferometry method can be found in Curtis et al. (2006).

Seismic noise interferometry can also be applied to frequencies larger than 1Hz. Schuster (2001) and Schuster et al. (2004) demonstrated the possibility of forming an image of the subsurface using the cross-correlation of seismic responses from natural and man-made sources at the surface or in the subsurface. Furthermore, within the context of exploration geophysics, Bakulin and Calvert (2004 and 2006) first proposed a practical application of seismic interferometry, showing that it is possible in practice to create a virtual source at a subsurface receiver location in a well. Other recent applications for the high-frequency range have been proposed by Dong and Schuster (2006) and Halliday et al. (2007) for surface-wave isolation and removal in active-source surveys. Among the several reasons that have stimulated the application of seismic noise interferometry to high frequencies, one is the possibility of applying this technique to suburban settings (Halliday et al., 2008), and another to exploit it for engineering seismology purposes, which require knowledge of the subsurface structure from depths of a few meters to several hundred meters.

The application of seismic noise interferometry to high frequencies is not merely a change of scale, since it involves also important questions still under discussion within the research community. For example, the effects of the high spatial and temporal variability in the distribution of noise sources occurring at high frequencies are still under investigation (Halliday and Curtis, 2008a and b), as well as the relationship between the wavelength of interest and inter-station distances. Several authors (e.g., Chavez-Garcia and Luzon, 2005; Chavez-Garcia and Rodriguez, 2007; Yokoi and Margaryan, 2008) showed, for a small scale experiment at a site with a homogeneous subsoil structure, the equivalence between the results obtained by cross-correlation in the time domain and the SPatial Auto-Correlation analysis (SPAC) method (Aki, 1957). However, it is worth noting that for non-homogeneous subsoil conditions, the SPAC method suffers a severe drawback. Indeed, as a general rule, such a method is used to retrieve the shallow soil structure below a small array of sensors by means of inversion of surface wave dispersion curves extracted by seismic noise analysis. Yet, the inversion is performed under the assumption that the structure below the site is nearly 1-D. Therefore, if the situation is more complicated (2-D or 3-D structure), then the SPAC method can only provide a biased estimate of the S-wave velocity structure. In contrast, one can expect that, similarly to what is obtained over regional scales, local heterogeneities will affect the noise propagation between sensors, and hence can be retrieved by analysing the Green's function estimated by the cross-correlation of the signals recorded at two different stations. For this reason, passive seismic interferometry is also believed to be a valuable tool for studying complex structures and performing surface wave tomography also for smaller

spatial scales of investigation. Picozzi et al. (2008) verified the suitability of seismic interferometry for seismic engineering and microzonation purposes. In fact, after having first evaluated the possibility of retrieving reliable and stable Green's functions within the limitations of time and instrumentation that bound standard engineering seismological experiments (for example, in urban microzonation studies, the number of deployed sensors is generally not larger than 20 and the acquisition time does not last more than a few hours), they applied the seismic interferometry technique to recordings from a 21-station array installed in the Nauen test site (Germany) (Yaramanci et al., 2002; and http://www.geophysik.tu-berlin.de/menue/forschung/testfeld_nauen/uebersicht). They showed that passive seismic interferometry is a valuable tool for the characterization of near-surface geology since the travel times estimated from the Green's functions analysis for different frequencies were inverted to derive the laterally varying 3-D surface wave velocity structure below the array, and with a few further steps the S-wave velocity structure as well. This represents a major innovation, due to the frequency range investigated and the scale of the experiment,

Figure 14.15 shows a 2-D cross section highlighting lateral velocity variations as inferred by seismic tomography from the application of seismic interferometry to seismic noise (Picozzi et al., 2008).
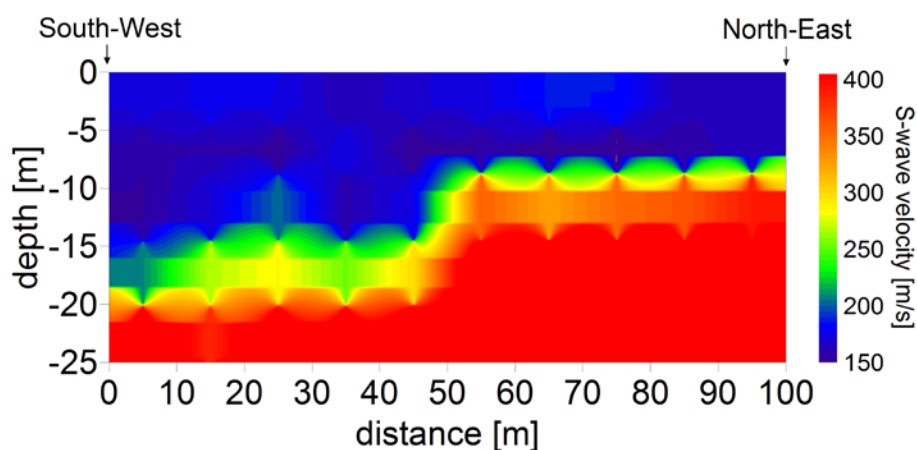

Fig. 14.15: S-wave velocity section extending southwest to northeast in the centre of the study area of Picozzi et al. (2008), derived by seismic noise tomography.

Furthermore, recent technical development (Picozzi et al., 2010b), show that in future it will be possible to overcome the problem of the high costs associated with of the application of this technique, caused by the large number of instruments required by using ad-hoc developed low-cost sensors.

14.6 Conclusions, suggestions and related case studies

Estimating site effects in large urban areas is a challenging task for seismologists and engineers. On the one hand, detailed site investigations are necessary for optimal design of buildings and foundations, while on the other hand urban planning and seismic risk mitigation actions could rely also on more general information about site amplification. Furthermore, the area that should be covered by related investigations for megacities might require large

investments and a long duration of the experiments. The rapid growth and expansion of populated areas, especially in developing countries, might even render the studies already outdated soon after their completion. A reasonable compromise between collection of empirical data at acceptable cost and within realistic time-frames can only be based on a mixed approach that combines the acquisition of high-quality (and thus high-cost) information at few sites with the application of rapid low-cost methods that allow for an extrapolation of the information over wide areas. With this aim, seismic microzonation of large urban areas can be carried out on the basis of site effect studies, which should involve:

1) Collection of all already available geological, geotechnical, and geophysical data.

2) Installation of a temporary seismic network for recording of earthquake data (about 3 months in duration). Local, regional and teleseismic events provide the necessary inputs for site effect estimation. The different frequency content of the recordings allows to cover the whole frequency range of engineering interest. The stations should be installed at characteristic sites taking into account the surface geology, topography and the expected depth variations of the bedrock surface.

3) Seismic noise recordings at single stations. Measurements should be carried out for at least 30 minutes at each site following the recommendation of SESAME (2003) (http://sesame-fp5.obs.ujf-grenoble.fr/SES_Home_Description.htm) and Picozzi et al. (2005a). In particular attention should be paid to the instruments used (Guiller et al., 2007; Strollo et al., 2008a and b). After calibration through comparison with earthquake data the fundamental resonance frequency estimated by NHV can be used for preparing maps. If an estimation of the thickness of the sedimentary layers is available, NHV can be inverted to derive S-wave velocity profiles. These, in turn, can be used to calculate 1-D site response or to generate 2-D and 3-D models that provide a basis for computing ground motion scenarios.

4) S-wave velocity profiles can be estimated using seismic noise arrays. .

Although these noise-based methods cannot be considered in general a substitute of investigation techniques dealing with active sources (that might provide more detailed information about the subsoil structure) they have the advantage to be easily applicable in urban areas (where method based on active sources might be impossible or suffer problems) and allow for investigating the subsurface structure down to large depths in a cost-effective way.

Tables 14.1 and 14.2 summarize essential points to be considered in the acquisition and analysis of earthquake data and seismic noise data, respectively, when carrying out such investigations. In the case that non-linear soil behaviour is likely this should be investigated by drilling of shallow boreholes and collection of undisturbed samples at a limited number of representative sites. If available funding allows for long-term monitoring, and improvement of estimates of site response for different levels of ground motion, the installation of vertical array of accelerometers should be considered. A similar combined approach was recently followed for different large urban areas. Parolai et al. (2004) installed a network of 40 seismological stations in the urban area of Cologne (Germany). Moreover they performed single station noise analysis at nearly 400 sites (Parolai et al., 2001b) and estimated the S-wave velocity at two sites by means of seismic noise array data analysis (Parolai et al. 2005; Parolai et al. 2006).

Parolai et al. (2010b) installed a network of 20 seismological stations in Bishkek and carried out single station noise measurements at nearly 200 sites (Figure 15.7).

Table 14.1 Suggestions for collection and analysis of earthquake data

Acquisition	- A sample rate of at least 100 s.p.s is suggested - Continuous recording allows to collect seismic noise and to record also regional and teleseismic events that might be masked by high frequency noise - Short period sensors might provide a reasonable compromise between the data quality and the temporary (low quality generally) installation.
Data analysis: window selection	The window length can be selected following different criteria: - fixed window lengths (be careful that all the significant part of ground motion is included); - window length selected on the base of energy criteria, e.g., including only part of signal containing 80% or 90% of the energy. Remember that frequency resolution is related to the total window length used. Since generally windows are tapered at both ends before the Fourier transform, the starting of the window should be selected in order to avoid that tapering is affecting the signal of interest. If, for example S waves are of interest, the window should start before the S-wave arrival.
Data analysis: Baseline correction, Tapering and smoothing	Removing the average of the signal might be necessary before calculating the Fast Fourier transform (FFT). Tapering at both ends is generally performed using windows. The percentage of tapering can vary. A generally used value is 5% of the signal length. The FFT of the signal should be smoothed, in order to avoid numerical instabilities. However, smoothing should allow to preserve the main features in the spectra. When spectra are spanning more than one decade it is preferable to smooth them using relative bandwidth windows.

Table 14.2 Suggestions for collection and analysis seismic noise data

Acquisition	- A sample rate of at least 100 s.p.s is recommended for single station noise measurements. Depending on the minimum inter-station distance, in the case of arrays, even larger sampling rates are suggested. - Short-period sensors might provide a reasonable compromise between high data quality and temporary installations of generally low data quality. - Please, check if the level of seismic noise is higher than the internal noise of the sensor+acquisition system in the frequency range of interest (see Chapter 5, section 5.5.6).
Data analysis: window selection	The windows should be selected keeping in mind the frequency band of interest. The maximum usable frequency is limited by the Nyquist frequency due to the sampling rate. The minimum frequency that can be analyzed is determined by the length of the selected signal window. However, stable results are expected only for frequencies that have a reasonable number of cycles (at least 10) within the selected signal window. In the case that the frequency range of interest spans between 0.1 and 10 Hz, window lengths of 20-60 seconds are suggested.
Data analysis: Baseline correction, tapering, smoothing and number of analysed windows.	Removing the average of the signal might be necessary before calculating the FFT. Tapering at both ends is generally performed using windows. The percentage of tapering can vary. A generally used value is 5% of the signal length. The FFT of the signal should be smoothed, in order to avoid numerical instabilities. However, smoothing should allow to preserve the main features in the spectra. When spectra are spanning more than one decade it is preferable to smooth them using relative bandwidth windows. When the frequency range of interest is 0.1-10 Hz at least 20 minutes of noise (divided in windows of 20-60 seconds) should be analysed.

Similarly, Picozzi et al. (2009), estimated the fundamental resonance frequency in western Istanbul (Turkey) by means of nearly 200 single station noise measurements. The reliability of the results was assessed by comparison with results from earthquake data obtained by analysing the recordings of the Istanbul Earthquake Rapid Response System (IERRS) operated by the Kandilli Observatory and Earthquake Research Institute of Bogazici University. Furthermore, eight 2-D array measurements of seismic noise were performed in the metropolitan area with the aim of obtaining a preliminary geophysical characterization of the different sedimentary covers. Comparison of the theoretical site response from an estimated S-wave velocity profile with the empirical one derived using earthquake recordings confirmed the suitability of the use of the low-cost seismic noise techniques for the study of seismic site effects.

Pilz et al. (2009) installed a temporary seismic network in Santiago de Chile (~6 million inhabitants). They estimate site amplification using the standard spectral ratio (SSR) method and proposed a map of the fundamental resonance frequency by analysing ~150 single station seismic noise recordings. Furthermore, by taking advantage of the available knowledge on bedrock depth from gravimetric measurements they derived a 3-D model of the basin that can be used for calculating realistic ground motion scenarios.

All these studies showed that the approach described above is feasible for covering large urban areas. at reasonable costs. Open questions still remain with respect to the estimation of a first order classification of soil that can be used, with a sufficient degree of reliability, at regional or even global scales.

Acknowledgment

References

Aki, K. (1957). Space and time spectra of stationary stochastic waves with special reference to microtremors. *Bull. Earthqu. Res. Inst.*, **35**, 415-456.

Aki, K. (1965). A note on the use of microseisms in determining the shallow structure of the Earth's crust. *Geophysics*, **30**, 665-666

Albarello, D., and Lunedei, E. (2009). Alternative interpretations of horizontal to vertical spectral ratios of ambient vibrations: new insights from theoretical modeling. *Bull. Earthq. Eng.*; doi: 10.1007/s10518-009-9110-0

Andrews, D. J. (1986). Objective determination of source parameters and similarity of earthquakes of different sizes. In: Das, S., Boatwright, J., and Scholz, C. H. (Editors), *Earthquake Source Mechanics*, American Geophysical Union, Washington D.C., 259–268.

Arai, H., and K. Tokimatsu (2000). Effects of Rayleigh and Love waves on microtremor H/V spectra, paper presented at *12th World Conference on Earthquake Engineering*, N. Z. Soc. for Earthquake Eng., Auckland, N. Z.

Arai, H., and K. Tokimatsu (2004). S-wave velocity profiling by inversion of microtremor H/V spectrum, *Bull. Seism. Soc. Am.* **94**, 53–63.

Assimaki, D., Li, W., Steidl, J. H., and Tsuda, K. (2008), Site amplification and attenuation via downhole array seismogram inversion: a comparative study of the 2003 Miyagi-Oki aftershock sequence. *Bull. Seism. Soc. Am.* **98**, 301-330.

Asten, M. W. (2006). On bias and noise in passive seismic data from finite circular array data processed using SPAC method. *Geophysics*, **71**, V153-V162, doi:10.1190/1.2345054.

Bakulin, A. and Calvert, R. (2004). Virtual source: new method for imaging and 4D below complex overburden. In: *Proceedings of 74th Annual International Meeting* (expanded abstracts), *Society of Exploration Geophysicists*, 2477–2480.

Bakulin, A. and Calvert, R. (2006). The virtual source method: theory and case study. *Geophysics,* 71, S1139–S1150.

Bard, P.-Y. (1995). Effects of surface geology on ground motion: recent results and remaining issues. In: *10th European Conference on Earthquake Engineering*, Duma (Editor), Balkema, Rotterdam, 305–323.

Bard, P.-Y. (1999). Microtremor measurements: A tool for site effect estimation? In: Irikura, K., Kudo, K., Okada, H., and Sasatani, T. (Eds.) (1999). The effects of surface geology on seismic motion. Proc. 2nd *International Symposium in Yokohama, Japan, 1-3 Dec. 1998, A. A. Balkema*, Rotterdam, ISBN 90 5809 030 2, 1251-1279.

Bindi, D., Parolai, S., Cara, F., Di Giulio, G., Ferretti, G., Luzi, L. , Monachesi, G. , Pacor, F., and Rovelli, A. (2009). Site amplifications observed in the Gubbio Basin, Central Italy: Hints for lateral propagation effects. *Bull. Seism. Soc. Am.*, **99**, 741-760.

Birtill, J. W., and Whiteway, F. E. (1965). The application of phased arrays to the analysis of seismic body waves. *Phil. Trans. R. Soc. of London, Math. and Phys. Sciences* **A-258,** No. 1091, 421-493.

Borcherdt, R. D. (1970). Effects of local geology on ground motion near San Francisco Bay. *Bull. Seism. Soc. Am.*, **60,** 29–61.

Bonilla, L. F., Steidl, J. H., Lindley, G. T., Tumarkin, A. G., and Archuleta, R. J. (1997). Site amplification in the San Ferdinando Valley, California: variability of site effect estimation using S-wave, coda, and H/V methods. *Bull. Seism. Soc. Am.*, **87,** 710–730.

Bonilla L.F., Archuleta R.J., and Lavallée, D. (2005). Hysteretic and dilatant behavior of cohesionless soils and their effects on nonlinear site response: Field data observations and modelling. *Bull. Seism. Soc. Am.*, **95**, 2373 - 2395.

Bonnefoy-Claudet S., Baize, S., Bonilla, L. F., Berge-Thierry, C., Pasten, C. R., Campos, J.,Volant, P., Verdugo, R. (2009). Site effect evaluation in the basin of Santiago de Chile using ambient noise measurements. *Geophys. J. Int*., **176** (3), 925–937.

Bormann, P. (1966). Recording and interpretation of seismic events (principles, present state and tendencies of development) (in German). *Publ. Inst. Geodyn.*, Jena, *Akademie Verlag*, Berlin, Vol. 1, 158 pp.

Campillo, M. and Paul, A. (2003). Long-range correlations in the seismic coda. *Science,* **299,** 547–549.

Capon, J. (1969). High-resolution frequency-wavenumber spectral analysis. *Proc. IEEE.*, 57, 1408-1419.

Castro, R. R., Anderson, J. G., and Singh, S. K. (1990). Site response, attenuation and source spectra of S-waves along the Guerrero, Mexico, subduction zone. *Bull. Seism. Soc. Am.* **80,** 1481–1503

Chavez-Garcıa, F. J. and Luzon, F. (2005). On the correlation of seismic microtremors. *J. Geophys. Res.*, **110**, B11313, doi:10.1029/2005JB003671

Chavez-Garcıa, F .J. and Rodrıguez, M. (2007). The correlation of microtremors: empirical limits and relations between results in frequency and time domains. *Geophys. J. Int.*, 171, 657–664.

Cho, K. H., Herrmann, R. B. and Ammon, C. J. and Lee, K. (2007). Imaging the upper crust of the Korean Peninsula by surface-wave tomography. *Bull. Seism. Soc. Am.,* **97**, 198–207, doi:10.1785/0120060096.

Curtis, A., Gerstoft, P., Sato, H., Snieder, R. and Wapenaar, K. (2006). Seismic interferometry - turning noise into signal. *Leading Edge*, **25**, 1082–1092.

D'Amico V., Picozzi M., Albarello D., Naso G. and Tropenscovino S. (2004). Quick estimate of soft sediments thickness from ambient noise horizontal to vertical spectral ratios: a case study in southern Italy". *J. Earthq. Engineering*, **8**, 6, 895-908.

D'Amico V., Picozzi M., Baliva F. and Albarello D. (2008). Ambient Noise Measurements for Preliminary Site-Effects Characterization in the Urban Area of Florence. *Bull.Seism.Soc.Am.,* **98**, 3, 1373-1388, doi: 10.1785/0120070231

Delgado, J., C. Lopez Casado, A. C. Estevez, J. Giner, A. Cuenca and S. Molina (2000a). Mapping soft soils in the Segura river valley (SE Spain): a case study of microtremors as an exploration tool, *J. Appl. Geophys.* **45,** 19–32.

Delgado, J., C. Lopez Casado, J. Giner, A. Estevez, A. Cuenca, and S. Molina. (2000b). Microtremors as a geophysical exploration tool: applications and limitations, *Pure Appl. Geophys.* **157,** 1445–1462. 1841.

Dong, S., He, R. and Schuster, G. (2006). Interferometric prediction and leastsquares subtraction of surface waves, in *Proceedings of 76th Annual International Meeting* (expanded abstracts), Society of Exploration Geophysicists, 2783–2786.

Douglas, A., (2002). Seismometer arrays – Their use in earthquake and test ban seismology, in *Handbook of Earthquake and Engineering Seismology*, edited by W. H. K. Lee, H. Kanamori, P. C. Jennings, and C. Kisslinger, 357-367, Academic Press, San Diego, California.

Drouet S., S. Chevrot, F. Cotton, and A. Souriau (2008). Simultaneous Inversion of Source Spectra, Attenuation Parameters, and Site Responses: Application to the Data of the French Accelerometric Network, *Bull. Seism. Soc. Am.*, **98**, 198 - 219.

Duval A.-M., S. Vidal, J.-P. Méneroud, A. Singer, F. De Santis, C. Ramos, G. Romero, R. Rodriguez, A. Pernia, N. Reyes and C. Griman (2001). Caracas, Venezuela, Site Effect Determination with Microtremors, *Pure and Applied Geophysiscs* **158**, 2513-2523

Fäh D, Kind F, Giardini D. (2001). A theoretical investigation of average H/V ratios. *Geophys. J. Int.* **145**, 535-549

Fäh, D., Kind, F. and Giardini, D. (2003). Inversion of local S-wave velocity structures from average H/V ratios, and their use for the estimation of site-effects. *J. Seismol.*, **7**, 449–467.

Field, E., and Jacob, K. H. (1993). The theoretical response of sedimentary layers to ambient seismic noise. *Geophys. Res. Lett.*,. **20**, 24, 2925-2928.

Field, E. H., and Jacob, K. H. (1995). A comparison and test of various site response estimation techniques, including three that are non reference- site dependent. *Bull. Seism. Soc. Am.*, **86,** 991–1005.

Field, E. H., Johnson, P. A., Beresnev, I. A., and Zeng, Y. (1997). Nonlinear ground-motion amplification by sediments during the 1994 Northridge earthquake. *Nature* **390**, 599-602.

Foti, S., Parolai, S., Albarello, D., Picozzi, M. (2011). Application of surface–wave methods for seismic site characterization. *Survey in Geophysics*, DOI 10.1007/s10712-011-9134-2.

Frosch, R. A., and Green, P. E. (1966). The concept of the large aperture seismic array, *Proc. R. Soc.*, London, Ser. A, **290**, 368-384.

Gerstoft P., Sabra, K. G., Roux, P., Kuperman, W. A. and Fehler, M. C. (2006). Green's functions extraction and surface-wave tomography from microseisms in southern California. *Geophysics,* **71**, 23–32.

Guiller B., Atakan, K., Chatelain, J.-L., Havskov, J., Ohrnberger, Cara, F., Duval, A.-M., Zacharopoulos, S., Teves-Costa, P., and the SESAME Team (2007). Influence of

instruments on the H/V spectral ratios of ambient vibrations. *Bull. Earth. Eng.*, **6**, 3-31. doi:10.1007/s10518-007-9039-0

Haghshenas, E., Bard, P.-Y., Theodulidis, N., and SESAME WP04 Team (2008). Empirical evaluation of microtremor H/V spectral ratio. *Bull. Earthquake Eng.*, doi: 10.1007/s10518-007-9058-x

Halliday D. F., and Curtis, A., (2008a). Seismic interferometry, surface waves, and source distribution. *Geophys. J. Int.*, doi:10.1111/j.1365- 246X.2008.03918.x.

Halliday D. F., and Curtis, A., (2008b). Seismic interferometry of scattered surface waves in attenuative media. *Geophys. J. Int.*, **178**, 419–446, doi: 10.1111/j.1365-246X.2009.04153.x.

Halliday D.F., Curtis A., Robertsson J.O.A. and van Manen D.-J. (2007). Interferometric surface-wave isolation and removal, *Geophysics,* 72, A67–A73.

Halliday D.F., Curtis A. and Kragh E., (2008). Seismic surface waves in a suburban environment - active and passive interferometric methods. *Leading Edge*, **27**, 210–218.

Harkrider, D. G, (1964). Surface waves in multilayered elastic media. I. Rayleigh and Love waves from buried sources in a multilayered elastic half-space. *Bull. Seism. Soc. Am.*, **54**, 627-679.

Horike, M. (1985). Inversion of phase velocity of long period microtremors to the S-wave velocity structure down to the basement in urbanized areas. *J. Phys. Earth* **33**, 59-96.

Hough S.E., Seeber L., Rovelli A., Malagnini L., DeCesare A., Selvaggi G., and Lerner-Lam A. (1992). Ambient noise and weak motion excitation of sediment resonances: results from the Tiber Valley, Italy. *Bull. Seism. Soc. Am.*, **82**, 1186-1205.

Ibs von Seht, M., and Wohlenberger, R. (1999). Microtremor measurements used to map thickness of soft soil sediments. *Bull. Seism. Soc. Am.*, **89**, 250-259.

Kárason, H., and van der Hilst, R.D. (2001). Tomographic imaging of the lowermost mantle with differential times of refracted and diffracted core phases (PKP, Pdiff), *J. Geophys. Res.*, **106**, 6569-6587.

Kind, F., Fäh, D., Giardini, D. (2005). Array measurements of S-wave velocities from ambient vibrations, *Geophysical Journal International*, **160**. 114-126.

Köhler, A., Ohrnberger, M., Scherbaum, F., Wathelet, M., and Cornou, C. (2007). Assessing the reliability of the modified three-component spatial autocorrelation technique. *Geophys J. Int.*, **168**, 779-796; doi:10.1111/j.1365-246X.2006.03253.x

Krüger, F., Baumann, M., Scherbaum, F., and Weber, M. (2001). Mid mantle scatterers near the Mariana slab detected with a double array method. *Geophys. Res. Lett.*, **28**, 667-670.

Kværna, T. (1989). On exploitation of small-aperture NORESS type arrays for enhanced P-wave detectability. *Bull. Seism. Soc. Am.*, **79**, 888-900.

Lachet, C., Hatzfeld, D., Bard, P.-Y., Theodulidis, N., Papaioannou, C., and Savvaidis, A. (1996). Site effects and microzonation in the city of Thessaloniki (Greece): comparison of different approaches. *Bull. Seism. Soc. Am.*, **86,** no. 6, 1692–1703.

Lacoss, R. T., Kelly, E.J., and Toksöz, M.N. (1969). Estimation of seismic noise structure using array. *Geophysics*, **29**, 21-38.

Langston, C. A. (1979). Structure under Mount Rainier, Washington, inferred from teleseismic body waves, *J. Geophys. Res.* **84,** 4749–4762.

Lermo, J. F., and Chavez-Garcia, F. J. (1993). Site effect evaluation using spectral ratios with only one station. *Bull. Seism. Soc. Am.* **83**, 1574-1594.

Lermo, J. F. and Chavez-Garcia, F. J., (1994). Are microtremors useful in site response evaluation?" *Bull. Seism. Soc. Am.*, **84**, 135, 1364.

Lin, F.-C., Ritzwoller, M.H., Townend, J., Bannister, S. and Savage M.K. (2007). Ambient noise Rayleigh wave tomography of New Zealand. *Geophys. J. Int.*, **170**, 649–666, doi:10.1111/j.1365–246X.2007.03414x.

Lobkins, O. I., and R .L. Weaver (2001). On the emergence of the Green's function in the correlation of a diffuse field. *Journal of Acoustical Society of America*, **110**, 3011-3017.

Louie, J. N. (2001). Faster, better: shear-wave velocity to 100 meters depth from refraction microtremor arrays. *Bull. Seismol. Soc. Amer.*, **91**, 2 , 347-364.

Lunedei, E., and Albarello, D. (2009). On the seismic noise wave field in a weakly dissipative layered Earth. *Geophys. J. Int.*;doi: 10.1111/j.1365-246X.2008.04062.x

Malagnini, L., Rovelli, A., Hough, S.E., and Seeber, L. (1993), Site amplification estimates in the Garigliano Valley, Central Italy, based on dense array measurements of ambient noise. *Bull. Seism. Soc. Am.*, **83**, 1744-1755.

Mehta, K., Snieder, R., and Grazier, V. (2007a). Extraction of near-surface properties for a lossy layered medium using the propagator matrix. *Geophys. J. Int.*, **169**, 2171-280.

Mehta, K., Snieder, R., and Grazier, V. (2007b). Downhole receiver function: a case study. *Bull. Seism. Soc. Am.*, **97**, 1396-1403.

Mogi H., S. M. Shrestha, H. Kawakami, and Shinya Okamura (2010). Nonlinear Soil Behavior Observed at Vertical Array in the Kashiwazaki-Kariwa Nuclear Power Plant during the 2007 Niigata-ken Chuetsu-oki Earthquake. *Bull. Seism. Soc. Am.*, **100**, 762-775.

Moya A., and Irikura, K. (2003). Estimation of Site Effects and Q Factor Using a Reference Event. *Bull. Seism. Soc. Am.*, **93**: 1730 - 1745.

Mucciarelli, M. (1998). Reliability and applicability of Nakamura's technique using micro-tremors: an experimental approach. *J. Earthq. Engrg.*, **2**, 625 638.

Nakamura, Y. (1989). A method for dynamic characteristics estimation of subsurface using microtremor on the ground surface. *Q. Rep. Railway Tech. Res. Inst.*, **30**, 25-33.

Nogoshi, M., and Igarashi, T. (1970). On the propagation characteristics of microtremors, *J. Seism. Soc. Japan*, **23,** 264–280 (in Japanese with English abstract).

Nogoshi, M., and Igarashi, T. (1971). On the amplitude characteristics of microtremor (part 2). *J. Seism. Soc. Japan*, **24**, 26-40 (Japanese with English abstract).

Ohori, M., Nobata, A., and Wakamatsu, K. (2002). A comparison of ESAC and FK methods of estimating phase velocity using arbitrarily shaped microtremor arrays. *Bull. Seism. Soc. Am.*, **92**, (6), 2323-2332.

Okada, H. (2003). The microtremor survey method. *Geophysical monograph series*, **12**, American Geophysical Union, Washington.

Oth, A., Bindi, D., Parolai, S., and Wenzel, F. (2008). S-wave attenuation characteristics beneath the Vrancea region in Romania: New insights from the inversion of ground-motion spectra. *Bull. Seism. Soc. Am.*, **98**, 2482-2497.

Oth, A., Parolai, S., Bindi, D., Wenzel, F. (2009). Source Spectra and Site Response from S Waves of Intermediate-Depth Vrancea, Romania, Earthquakes. *Bull. Seism. Soc. Am.*, **99**, 235-254.

Park C. B., Miller R. D., and Xia J. (1999). Multichannel analysis of surface waves. *Geophysics*, **64**, 800-808.

Parolai, S., and Richwalski, S. M. (2004). The importance of converted waves in comparing H/V and RSM site responses. *Bull. Seism. Soc. Am.*, **94,** 304–313.

Parolai, S., and Galiana-Merino, J. J. (2006): Effect of transient seismic noise on estimates of H/V spectral ratios. *Bull. Seism. Soc. Am.*, **96**, 1, 228-236.

Parolai, S., Bindi, D., and Augliera, P. (2000). Application of the Generalized Inversion Technique (GIT) to a microzonation study: numerical simulations and comparison with different site-estimation techniques. *Bull. Seism. Soc. Am.*, **90,** no. 2, 286–297.

Parolai, S., Trojani, L., Monachesi, G., Frapiccini, M., Cattaneo, M., and Augliera, P. (2001). Hypocenter location accuracy and seismicity distribution in the Central Apennines (Italy). *J. Seism.*, **5**, 243-261.

Parolai, S., Bindi, D., and Troiani, L. (2001a). Site response for the RSM seismic network and source parameters in the Central Apennines (Italy). *Pure Appl. Geophys.*, **158,** 695–715.

Parolai S, Bormann, P, and Milkereit, C. (2001b). Assessment of the natural frequency of the sedimentary cover in the Cologne area (Germany) using noise measurements. *J. Earthq. Engrg.*, **5,** 541-564.

Parolai S, Bormann, P, Milkereit, C. (2002). New relationships between V_s, thickness of sediments, and resonance frequency calculated by the H/V ratio of seismic noise for the Cologne area (Germany). *Bull. Seism. Soc. Am.*, **92,** 2521-2527.

Parolai S, Richwalski, S. M, Milkereit, C, and Bormann, P. (2004). Assessment of the stability of H/V spectral ratio from ambient noise and comparison with earthquake data in the Cologne area (Germany). *Tectonophysics*, **390**, 57-73.

Parolai, S., Picozzi, M., Richwalski, S. M., and Milkereit, C. (2005). Joint inversion of phase velocity dispersion and H/V ratio curves from seismic noise recordings using a genetic algorithm, considering higher modes. *Geoph. Res. Lett.*, **32**, doi: 10.1029/2004GL 021115

Parolai, S., Richwalski, S. M., Milkereit, C., and Fäh, D. (2006). S-wave velocity profiles for earthquake engineering purposes for the Cologne area (Germany). *Bull. Earth. Engineering*, **4**, 65-94.

Parolai, S., Grünthal, G., and Wahlström, R., (2007). Site-specific response spectra from the combination of microzonation with probabilistic seismic hazard assessment - An example for the Cologne (Germany) area. *Soil Dynamics and Earthquake Engineering*, **27**, 1, 49-59.

Parolai, S., Bindi, D., Durukal, E., Grosser, H., and Milkereit, C. (2007). Source parameter and seismic moment-magnitude scaling for northwestern Turkey. *Bull. Seim. Soc. Am.*, **97**(2), 655-660.

Parolai, S., Ansal, A., Kurtulus, A., Strollo, A., Wang, R., and Zschau, J. (2009). The Ataköy vertical array (Turkey): insights into seismic wave propagation in the shallow-most crustal layers by waveform deconvolution. *Geophys. J. Int*; doi:10.1111/j.1365-246X.2009.04257. x

Parolai S., Bindi, D., Ansal, A., Kurtulus, A., Strollo, A. and Zschau, J. (2010a). Determination of shallow S-wave attenuation by down-hole waveform deconvolution: a case study in Istanbul (Turkey). *Geophys. J. Int*., doi: 10.1111/j.1365-246X.2010.04567.x

Parolai S., Orunbaev, S., Bindi, D., Strollo, A., Usupaev, S., Picozzi, M., Di Giacomo, D., Augliera, P., D'Alema, E., Milkereit, C., Moldobekov, B., and Zschau, J. (2010b). Site effect assessment in Bishkek (Kyrgyzstan) using earthquake and noise recording data. *Bull. Seism. Soc. Am.*, **100**, 3068-3082.

Picozzi, M. (2006). Joint inversion of phase velocity dispersion and H/V ratio curves from seismic noise recordings. *PhD. Thesys, University of Siena*, 170 pp.

Picozzi, M., Parolai, S., and Albarello, D. (2005a). Statistical analysis of noise horizontal to-vertical spectral ratios (HVSR). *Bull. Seism. Soc. Am.*, **95**,1779,1786.

Picozzi, M., Parolai, S., and Richwalski, S. M. (2005b). Joint inversion of H/V ratios and dispersion curves from seismic noise: Estimating the S-wave velocity of bedrock. *Geoph. Res. Lett.*, **32**, doi: 10.1029/2005GL022878.

Picozzi, M., and Albarello, D.(2007). Combining genetic and linearized algorithms for a two-step joint inversion of Rayleigh wave dispersion and H/V spectral ratio curves. *Geophys. J. Int.*, **169**, 189–200.

Picozzi, M., Parolai, S., Bindi, D., Strollo, A. (2008). Characterization of shallow geology by high-frequency seismic noise tomography. *Geophysical Journal International*, **176**, 1, 164-174.

Picozzi, M., Strollo, A., Parolai, S., Durukal, E., Özel, O., Karabulut, S., Zschau, J., Erdik, M. (2009). Site characterization by seismic noise in Istanbul, Turkey. *Soil Dynamics and Earthquake Engineering*, **29**, 3, 469-482.

Picozzi, M., Parolai, S., and Bindi, D. (2010a): Deblurring of frequency-wavenumber images from small-scale seismic arrays. *Geophys.l J. Internat.*; doi: <u>10.1111/j.1365-246X.2009. 04471.x</u>

Picozzi, M., Milkereit, C., Parolai, S., Jaeckel, K.-H., Veit, I., Fischer, J., Zschau, J. (2010b). GFZ Wireless Seismic Array (GFZ-WISE), a wireless mesh network of seismic sensors: New perspectives for seismic noise Aaray investigations and site monitoring. *Sensors*, **10**(4), 3280-3304.

Pilz, M., Parolai, S., Leyton, F., Campos, J., and Zschau, J. (2009). A comparison of site response techniques using earthquake data and ambient seismic noise analysis in the large urban areas of Santiago de Chile. *Geophys. J. Internat.*, **178**, 2, 713-728.

Pilz, M., Parolai, S., Picozzi, M., Wang, R., Leyton, F., Campos, J., and Zschau, J. (2010). Shear wave velocity model of the Santiago de Chile basin derived from ambient noise measurements: a comparison of proxies for seismic site conditions and amplification. *Geophys. J. Internat., ***182,*** 355-367.

Riepl, J., Bard, P.-Y., Hatzfeld, D., Papaioannou, C., and Nechtschein, S. (1998). Detailed evaluation of site response estimation methods across and along the sedimentary valley of Volvi (EURO-SEISTEST). *Bull. Seism. Soc. Am.*, **88,** no. 2, 488–502.

Ritter, J. R. R., Jordan, M., Christensen, U., and Achauer, U. (2001). A mantle plume below the Eifel volcanic fields, Germany. *Earth Planet. Sci. Lett.*, **186**, 7-14.

Rost, S., and Thomas, C. (2002). Array Seismology: Methods and applications. *Rev. Geophys.*, **40** (3), 1008, doi: 10.1029/20000RG000100.

Sabra, K.G., Gerstoft, P., Roux, P., Kuperman, W.A., and Fehler, M.C. (2005). Surface wave tomography from microseisms in Southern California. *Geophys. Res. Lett.,* **32**, L14311, doi:10.1029/2005GL023155.

Safak, E. (1997). Models and methods to characterize site amplification from a pair of records. *Earthquake Spectra*, EERI, **13**, 97-129.

Safak, E. (2001). Local site effects and dynamic soil behaviour. *Soil Dynamics and Earthquake Engineering*, Elsevier Science Ltd., Vol. 21, pp.453-458**.**

Scherbaum, F., Hinzen, K.G., and Ohrnberger, M. (2003). Determination of shallow shear wave velocity profiles in the Cologne, Germany, area using ambient vibrations. *Geophys. J. Int.*, **152**, 597-612.

Schuster, G. T. (2001). Theory of daylight/interferometric imaging: tutorial. In: *Proceedings of 63rd Meeting, European Association of Geoscientists and Engineers*, Session: A32 (extended Abstracts).

Schuster, G. T., Yu, J., Sheng, J., and Rickett, J. (2004). Interferometric/daylight seismic imaging. *Geophy. J. Int.*, **157**, 838-852.

SESAME group (2003). Final report on measurements guidelines, LGIT Grenoble, CETE Nice,WP02,H/V technique:experimental conditions, [http://sesame-fp5.obs.ujf-grenoble.fr/ Delivrables/D08-02_Texte.pdf](http://sesame-fp5.obs.ujf-grenoble.fr/Delivrables/D08-02_Texte.pdf)

Shapiro, N. M, and Campillo, M. (2004). Emergence of broadband Rayleigh waves from correlations of ambient seismic noise. *Geophys. Res. Lett.*, **31**, L07614, doi10.1029/2004GL019491.

Shapiro, N. M., Campillo, M., Stehly, L., and Ritzwoller, M. (2005). High resolution surface wave tomography from ambient seismic noise. *Science,* 307, 1615–1618

Snieder, R. (2004). Extracting the Green's function from the correlation of coda waves: a derivation based on stationary phase. *Phys. Rev. E,* **69**; doi:10.1103/PhysRevE.69.046610.

Snieder, R.(2006). The theory of coda wave interferometry. *Pure Appl. Geophys.*, **163**, 455-473.

Snieder, R., Sheiman, J., and Calvert, R. (2006). Equivalence of the virtual-source method and wave-field deconvolution in seismic interferometry. *Physical Review E*, **73**, 066620.

Steidl, J. H., Tumarkin, A. G., and Archuleta, R. (1996). What is a reference site? *Bull. Seism. Soc. Am.*, **86,** no. 6, 1733–1748.

Stokoe K. H. II, Wright, S. G., Bay, J.A., Roesset, J.M.(1994). Characterization of geotechnical sites by SASW method. In: R.D. Woods (Ed.), *Geophysical Characterization of Sites*, 15-25.

Strollo A., D. Bindi,, S. Parolai,, K.-H. Jäckel (2008a). On the suitability of 1 s geophone for ambient noise measurements in the 0.1–20Hz frequency range: experimental outcomes, *Bulletin of Earthquake Engineering*, **6**, 1, 141-147.

Strollo, A., Parolai, S., Jäckel, K.-H., Marzorati., S., and Bindi, D. (2008b). Suitability of short-period sensors for retreiving reliable H/V peaks for frequencies less than 1 Hz. *Bull. Seism. Soc. Am.*, **98**, 2, 671-681.

Tada, T., Cho, I., Shinozaki, Y. (2006). A two-radius circular array method: inferring phase velocity of Love waves using microtremor records. *Geophys. Res. Lett*, **33**, L10303; doi:10.1029/2006GL025722.

Trampert, J., Cara, M., and Frogneux, M. (1993). SH propagator matrix and Qs estimates from borehole- and surface-recorded earthquake data. *Geophy. J. Int*., **112,** 290-299**.**

Triantafyllidis, P., Hatzidimitriou, P. M., Theodulidis, M., Suhadolc, P., Papazachos, C., Raptakis, D., and Lontzetidis, K. (1999). Site effects in the city of Thessaloniki (Greece) estimated from acceleration data and 1D local soil profiles. *Bull. Seism. Soc. Am.*, **89,** 521–537.

van Vossen, R., Trampert, J., and Curtis, A. (2004). Propagator and wave-equation inversion for near-receiver material properties. *Geophy. J. Int*., **157,** 796-812**.**

van Vossen, R., Curtis, A., and Trampert, J. (2005). Subsonic near-surface P-velocity and low S-velocity observation using propagator inversion. *Geophysics***, 70**, R15-R23.

von Kamp, H. (1986). Geologische Karte von Nordrhein-Westfalen 1:100.000. *Geologisches Landesamt Nordrhein-Westfalen*, Germany.

Wapenaar, K. (2004). Retrieving the elastodynamic Green's function of an arbitrary inhomogeneous medium by cross correlation. *Phys. Rev. Lett.,* **93**, 25 4301–1-4.

Wapenaar, K., and Fokkema, J. (2006). Green's function representations for seismic interferometry. *Geophyscis*, **71**, SI33–SI44.

Weaver, R., and Lobkis, O. (2001). On the emergence of the Green's function in the correlations of a diffuse field. *J. acoust. Soc. Am.*, **109**, 2410.

Weaver, R. L., and Lobkis, O. I. (2004). Diffuse fields in open systems and the emergence of the Green's function. *J. acoust. Soc. Am.*, **116**, 2731–2734.

Whiteway, F.E. (1966). The use of arrays for earthquake seismology. *Proc. R. Soc. London*, Ser. A, **290**, 328-348.

Yamada, M., Mori, J., and Ohmi, S. (2010). Temporal Changes of Subsurface Velocities during Strong Shaking as Seen from Seismic Interferometry. *J. Geophys. Res.*, **115**, B03302, doi:10.1029/2009JB006567.

Yamanaka, H., Takemura, M., Ishida, H., and Niwa, M. (1994). Characteristics of long-period microtremors and their applicability in the exploration of deep sedimentary layers. *Bull. Seism. Soc. Am.*, **84,** 1831–1841.

Yang, Y., Ritzwoller, M. H., Levshin, A.L., and Shapiro, N. M. (2007). Ambient noise Rayleigh wave tomography across Europe. *Geophys. J. Int.,* **168**, 259–274, doi:10.1111/j.1365–246X.2006.03203.x

Yao, H., Van Der Hilst, R. D., and De Hoop, M.V. (2006). Surface-wave array tomography in SE Tibet from ambient seismic noise and two station analysis: I - phase velocity maps. *Geophys. J. Int.,* **166**, 732– 744.

Yaramanci, U., Lange, G., and Hertrich, M. (2002). Aquifer characterisation using Surface NMR jointly with other geophysical techniques at the Nauen/Berlin test site *J. Appl. Geophys.,* **50**, 47–65.

Zhang, S. H., Chan, L. S., and Xia, J. (2004). The selection of field acquisition parameters for dispersion images from multichannel surface wave data. *Pure Appl. Geophys.*, **161**, 185–201

Zywicki, D. J. (1999). Advanced signal processing methods applied to engineering analysis of seismic surface waves. PhD thesis at Georgia Institute of Technology